Redox Biology 40 (2021) 101842

Contents lists available at ScienceDirect

Redox Biology

journal homepage: www.elsevier.com/locate/redox

Research Paper

RhoA GTPase phosphorylated at tyrosine 42 by src kinase binds to β-catenin and contributes transcriptional regulation of vimentin upon Wnt3A

Jae-Gyu Kim [a,b,*], Shohel Mahmud [a,g], Jung Ki Min [a], Yoon-Beom Lee [a], Hyunbin Kim [e], Dong-Chul Kang [f], Hwee-Seon Park [a], Jihye Seong [e,h], Jae-Bong Park [a,b,c,d,**]

[a] Department of Biochemistry, Hallym University College of Medicine, Hallymdaehag-Gil 1, Chuncheon, Kangwon-Do, 24252, Republic of Korea
[b] Institute of Cell Differentiation and Aging, College of Medicine, Chuncheon, Kangwon-do, 24252, Republic of Korea
[c] Hallym Clinical and Translational Science Institute, Republic of Korea
[d] ELmed Co. Room 3419, Hallym University, Chuncheon, Kangwon-do, 24252, Republic of Korea
[e] Convergence Research Center for Diagnosis Treatment Care of Dementia, Korea Institute of Science Technology (KIST), Seoul, 02792, Republic of Korea
[f] Ilsong Institute of Life Science, Hallym University, Anyang-si, 14066, Republic of Korea
[g] National Institute of Biotechnology, Ganakbari, Ashulia, Savar, Dhaka, 1349, Bangladesh
[h] Brain Science Institute, Korea Institute of Science and Technology, Seoul, 02792, Republic of Korea

ARTICLE INFO

Keywords:
p-Tyr42 RhoA
β-Catenin
Wnt3A
Superoxide
GSK-3β
Src
Cancer

ABSTRACT

In the Wnt canonical pathway, Wnt3A has been known to stabilize β-catenin. In the non-canonical Wnt signaling pathway, Wnt is known to activate Rho GTPases. The correlation between canonical and non-canonical pathways by Wnt signaling, however, has not been well elucidated. Here, we identified that Wnt3A promoted superoxide generation, leading to Tyr42 phosphorylation of RhoA through activations of *c*-Src and Rho-dependent coiled coil kinase 2 (ROCK2) and phosphorylation of p47phox, a component of NADPH oxidase. Wnt3A also induced accumulation of β-catenin along with activations of RhoA and ROCK1. Concurrently, ROCK1 was able to phosphorylate GSK-3β at Ser9, which phosphorylated Src at Ser51 and Ser492 residues, leading to Src inactivation through dephosphorylation of Tyr416 during the late period of Wnt3A treatment. Meanwhile, *p*-Tyr42 RhoA bound to β-catenin via the *N*-terminal domain of β-catenin, thereby leading to the nuclear translocation of *p*-Tyr42 RhoA/β-catenin complex. Notably, *p*-Tyr42 RhoA as well as β-catenin was associated with the promoter of *Vim*, leading to increased expression of vimentin. In addition, stomach cancer patients harboring higher expressed *p*-Tyr42 Rho levels revealed the much poorer survival probability. Therefore, we propose that *p*-Tyr42 RhoA is crucial for transcriptional regulation of specific target genes in the nucleus by binding to their promoters and involved in tumorigenesis.

1. Introduction

Wnt signaling regulates a wide variety of biological processes including cell proliferation, differentiation, polarity, survival, and migration for developmental and tumorigenic events. Wnt signaling could be classified into two pathways, namely the canonical transforming β-catenin-dependent and the non-canonical non-transforming β-catenin-independent pathways [1]. In absence of Wnt signaling, glycogen synthase kinase-3 β (GSK-3β) phosphorylates β-catenin in a 'destruction complex'. This complex is made up of GSK-3β, adenomatous polyposis coli (APC), Axin, β-catenin and casein kinase I (CKI), where CKI primes the phosphorylation of β-catenin's Thr45 residue and GSK-3β then subsequently phosphorylates Ser41, Ser37, and Ser33 of β-catenin, leading to β-catenin degradation by 26 S proteasome [1].

In presence of Wnt, there is the stimulation of cells in the canonical pathway as GSK-3β phosphorylates lipoprotein receptor-related protein 6 (LRP6) rather than β-catenin, which is necessary for Axin to bind to LRP6 together with GSK-3β and APC [2]. With Wnt stimulation, phosphorylated *N*-terminus of LRP6 binds to GSK-3β, resulting in inhibition of GSK-3β′s ability to phosphorylate β-catenin [3]. Thus, β-catenin is then released from GSK-3β, leading to increased β-catenin stability and

* Corresponding author. Department of Biochemistry, Hallym University College of Medicine, Hallymdaehag-Gil 1, Chuncheon, Kangwon-Do, 24252, Republic of Korea.
** Corresponding author. Department of Biochemistry, Institute of Cell Differentiation and Aging, Hallym University, Chuncheon, Kangwon-do, 24252, Republic of Korea.
E-mail addresses: mip11@hallym.ac.kr (J.-G. Kim), jbpark@hallym.ac.kr (J.-B. Park).

https://doi.org/10.1016/j.redox.2020.101842
Received 17 October 2020; Received in revised form 17 December 2020; Accepted 17 December 2020
Available online 25 December 2020

Abbreviations

Apo	Apocynin
CK1	casein kinase 1
Daam	Dvl associated activator of morphogenesis
Dvl	disheveled
EMT	epithelial mesenchymal transition
GEF	guanine nucleotide exchange factor
GSK-3β	glycogen synthase kinase-3β
LPA	lysophophatidic acid
LRP	lipoprotein receptor-related protein
Luc	luciferase
NAC	N-acetyl cysteine
NRX	nucleoredoxin
NTD	N-terminal domain
ROCK	Rho-dependent coiled coil kinase
PKB	protein kinase B
TCF	T-Cell-Specific Transcription Factor
WGEF	weak-similarity GEF

accumulation in the cytosol and nucleus [4].

Several other stimuli have also been documented to inactivate GSK-3 and in the insulin signaling pathway, inhibition of GSK-3 activity has been well documented [5,6]. With insulin stimulating phosphatidylinositol-3-kinase (PI3K), protein kinase B (PKB)/Akt is in turn activated, which then phosphorylates the GSK isoforms (Ser9 of GSK-3β and Ser21 of GSK-3α), leading to inactivation of GSK-3β [5,6]. In certain cancer cells, AKT/PKB/GSK-3β phosphorylation regulates β-catenin levels by either insulin or Wnt1 [7,8]. However, the accumulation of β-catenin by Wnt1 is not via phosphorylation of GSK-3β′s Ser9 [9]. In addition, Wnt3A stabilizes β-catenin along with phosphorylation of GSK-3β at Ser9; however, this GSK-3α/β phosphorylation is not essential for β-catenin stabilization [10]. These reports reveal evidence that β-catenin stabilization can occur dependently or independently of GSK-3β Ser9 phosphorylation, depending on the stimulus and cell type. Overall, the functional regulatory mechanism of *p*-Ser9 GSK-3β has not been well understood in Wnt signaling pathway.

Wnt5A is a ligand for non-canonical Wnt signaling and it regulates cytoskeleton and cellular polarity during development and also tissue homeostasis as part of the Wnt/planar cell polarity (PCP) pathway [11,12]. Upon Wnt ligand binding, the Wnt receptor Frizzled binds to Disheveled (Dvl) protein, which then associates with Rho-GTPases [13,14] via the formin homology adaptor protein, Daam1 (Dvl associated activator of morphogenesis 1) [12,15].

As a small GTPase, RhoA can be activated by several guanine nucleotide exchange factors (GEFs) resulting in GTP binding to RhoA, representing an activated RhoA. Conversely, RhoA can be inactivated by GTPase activating proteins (GAPs) which catalyze GTP hydrolysis, leading to a GDP-bound RhoA, which is inactive. The inactive RhoA-GDP is localized in the cytosol in a complex with Rho guanine nucleotide dissociation inhibitor (RhoGDI) and active RhoA-GTP is localized in the membrane via linkage through geranylgeranyl group covalently bound to the Cys residue in the *C*-terminus of RhoA. It is notable that IKKγ (also known as NEMO) facilitates RhoA activation via IKKγ (NEMO) causing the dissociation of the RhoA-RhoGDI complex [16]. Active RhoA-GTP binds to its effector proteins including Rho-associated coiled coil kinase (ROCK), thereby transmitting its signals to downstream signaling pathways [17]. In particular, Tyr42 of RhoA phosphorylated by *c*-Src binds to IKKγ, leading to IKKβ activation, IκB phosphorylation and its degradation, resulting in NF-κB activation and tumorigenesis [18]. Recently, Tyr42 of RhoA was reported to be also phosphorylated by c-Met tyrosine kinase in gastric cancer cells [19]. In non-canonical Wnt signaling, the RhoA pathway comes into play as Dvl protein and the activated Daam1 bind to WGEF (weak-similarity GEF), a Rho GEF, thus promoting formation of RhoA-GTP, which then induces activation of ROCK and the resultant dynamic cytoskeletal rearrangements [20].

Interestingly, Wnt3A induces both the canonical β-catenin-dependent signaling and the non-canonical Rho-GTPase-mediated signaling [21–24]. Furthermore, β-catenin and Rho can cooperate to regulate the transcriptional induction of Wnt3A target CTGF, although neither β-catenin stabilization nor the nuclear translocation of β-catenin by Wnt3A was affected by RhoA [25]. In addition, β-catenin accumulation is governed by RhoA activity in response to Wnt3A. Notably, ROCK1 phosphorylates Ser9 of GSK-3β [26]. Nonetheless, the molecular mechanism between β-catenin accumulation and RhoA activity by Wnt3A has not been clarified.

In this study, we found that Wnt3A induces interaction of *p*-Tyr42 RhoA and β-catenin and *p*-Tyr42 RhoA delivers β-catenin to the nucleus, where *p*-Tyr42 RhoA as well as β-catenin regulates expression of specific genes such as *Vim* by binding to *Vim* promoter. Notably, ROCK1-mediated *p*-Ser 9 GSK-3β, which has been known to be inactive form, was able to phosphorylate Ser51/493 of Src, resulting in Src inactivation for desensitization of Wnt3A stimulation.

2. Materials and methods

2.1. Cell culture

Human kidney embryonic cell line (HEK293T) were cultured in Dulbecco's modified eagle medium-F12 (DMEM-F12; Lonza, Basel, Switzerland) containing 5% fetal bovine serum (FBS; GIBCO, Carlsbad, USA) and 1% penicillin-streptomycin (complete media) at 37 °C and 5% CO_2. Cell proliferation was measured using MTT assay (Biomax QM1000, Biomax Research Institute Co. Seoul, Korea).

2.2. Western blotting

HEK293T cells were collected and washed with ice-cold PBS, and lysed with RIPA buffer (50 mM Tris-HCl (pH7.4), 150 mM NaCl, 1% Nonidet P-40, 0.25% NaN_3, 1 mM EDTA, 1 mM PMSF, 1 μg/ml aprotinin, 1 μg/ml leupeptin, 1 μg/ml pepstatin, 1 mM sodium orthovanadate, and 1 mM NaF). The cell lysates were centrifuged for 20 min at 13,475×*g* and the supernatants were analyzed for protein concentration using BCA Protein Assay kit (Pierce; Rockford, USA). The proteins of cell lysates were run on SDS-PAGE, and transferred to PVDF membrane (Millipore; Billerica, USA). *Anti*-RhoA (1/500), anti-actin (Santa Cruz; Dallas, CA), *anti*-GSK-3β (1/500), *anti*-phospho (Ser9)-GSK-3β (1/500) (both from Cell Signaling, Beverly, USA), *anti*-β-catenin (1/1000) (Invitrogen; Carlsbad, USA), anti-active β-catenin (1/500) (Millipore; Billerica, USA), and anti-Tau (1/500) (Biosource; Camarillo, CA) antibodies were incubated with a PVDF membrane for 2 h at room temperature, and then washed three times for 5 min each. The membrane was then incubated was incubated for 1 h with anti-rat IgG or anti-mouse IgG antibody conjugated with horse radish peroxidase (HRP) (both from ENZO Life Science; Farmingdale, USA) (1/1000 diluted) and later washed three times for 10 min each. The membrane was incubated with enhanced chemiluminescence (ECL) reagents (Amersham; Uppsala, Sweden), and then identified by Gel documentation system. The intensity of the bands was quantified by ImageJ program from the U.S. National Institutes of Health (Bethesda, USA) [27].

2.3. Immunoprecipitation (IP)

Cells at 1×10^7 were washed with 1 × PBS and the cell lysates were prepared using a cell lysis buffer (20 mM Tris pH 7.4, 120 mM NaCl, 1% Nonidet P-40) containing 10 μg/ml each of leupeptin, aprotinin and 1 mM each of NaF, Na_3VO_4, PMSF plus 5 mM $MgCl_2$. The lysates were then used for immunoprecipitation by specific antibodies [28].

2.4. Purification of recombinant GST-β-catenin fusion protein and Tat-C3 toxin

Recombinant GST-β-catenin was expressed in *E. coli* using pGEX-4T1 host vector. The protein expression was induced by adding 0.5 mM isopropylthio-galactosidase (IPTG) to the transformed culture of *E. coli* BL21. The GST-β-catenin fusion protein was purified using glutathione (GSH)-Sepharose 4B beads. Recombinant His-tagTat-C3 exoenzyme was purified from *E. coli* by using Ni^{+}-beads [28].

2.5. In vitro kinase assay of ROCK2

To determine the phosphorylation of GSK-p47phox by ROCK2, 100 ng of active ROCK2 (amino acids, aa 17–535) and 100 ng of recombinant GST-p47phox were mixed and incubated for 30 min at 30 °C in 40 μl of the kinase assay buffer (10 mM HEPES (pH 7.5), 50 mM glycerolphosphate, 50 mM NaCl, 10 mM $MgCl_2$, 10 mM $MnCl_2$, 1 mM DTT, 30 μM ATP), and the samples were incubated for 30 min at 30 °C. The samples were analyzed by Western blot using *anti-p*-Ser345 p47phox antibody [16].

2.6. Si-RNA and sh-RhoA plasmid transfection

The short-hairpin (sh)-RNA expression sequence for targeting RhoA mRNA was cloned into the pSUPER RNAi vector (Oligoengine; Seattle, USA) (Moon et al., 2013; Shimizu et al., 2007). Transfection of RAW 264.7 cells with small interference (si)-RNA or sh-RhoA plasmid was performed using HiPerFect(QIAGEN) transfection reagent. *Si*-RNA (100 ng/ml) or sh-RhoA plasmid (2 μg/ml) in 100 μl culture medium without serum was mixed with 3 μl of HiPerFect transfection reagent for 10 s with vortexing, and incubated for 5–10 min at room temperature. The mixture was then added drop-wise onto the cells in 5 ml serum-free media. After 4–5 h, 8×10^5 cells were cultured in 60 mm dish of 5 ml appropriate culture medium containing serum and antibiotics at 37 °C and 5% CO_2 [29].

2.7. Pull-down assay

RhoA activity was detected using the EZ-Detect™ Rho activation kit (Pierce; Rockford, USA) according to the manufacturer's instruction. The cells were stimulated with Wnt3A (30 ng/ml); they were then collected, washed once with cold PBS, and then lysed in a buffer of 25 mM Tris-HCl (pH7.4), 150 mM NaCl, 5 mM $MgCl_2$, 1% NP-40, 1 mM DTT, 5% glycerol, 1 μg/ml aprotinin, 1 μg/ml leupeptin and 1 mM PMSF. The samples were incubated on ice for 5 min, followed by centrifugation (16,000×*g*, 15 min, 4 °C). Equivalent amounts of protein from the supernatants were then incubated with GST-Rhotekin-RBD for GTP-RhoA (Pierce). The beads were washed 5 times with the lysis buffer and bound proteins were eluted with 2 x Laemmli sample buffer by boiling. The samples were electrophoresed and analyzed by Western blotting with *anti*-RhoA antibody. As a control experiment, GDP (1 mM) or GTPγS (0.1 mM) was incubated with the cell lysates (1 mg/ml, 500 μl) in presence of 10 mM EDTA for 30 min at 30 °C; then, 60 mM $MgCl_2$ was added to maintain GDP/GTPγS-binding to GTPases. RhoA-GTP levels in the samples were then determined [16].

2.8. Top-flash luciferase reporter gene assay

Cells growing to 80% confluence in a 35 mm culture dish were transfected with β-catenin/T-cell factor (TCF)/lymphoid enhancer factor (LEF) reporter plasmid (Top-flash luciferase reporter plasmid, M50 Super8X Top-flash; Clontech, 2 μg) and pCMV-β-GAL (2 μg), an expression plasmid for *E. coli* β-galactosidase (for transfection level calibration). Twenty-four hours after the transfection, the cells were treated with 30 ng/ml Wnt3A. The cells were lysed in the lysis buffer (Reporter Lysis buffer) (Promega; Madison, USA) and cell debris was removed by centrifugation. The supernatant was used for measuring the relative luciferase activity according to the manufacturer's instruction (Promega Dual-Luciferase Reporter Assay system E1910) in a luminometer (Lumat LB 9057, EG and G Berthold; Wildbad, Germany).

2.9. Confocal microscopy

Cells were cultured and treated with Wnt3A (20 ng/ml). The cells were then fixed with 4% paraformaldehyde for 10 min, neutralized with 20 mM glycine for 10 min, and then washed three times with PBS containing 0.1% Triton X-100 (T-PBS). The samples were incubated with the specified primary antibody (1:100) overnight at 4 °C, washed, and then incubated with the *anti*-β-catenin antibody which was then recognized by an Alexa Fluor 488-conjugated secondary antibody (green-color emission) for 2 h at 24 °C. DAPI (1 μg/ml) was also added 10 min before washing to label the nuclei. Fluorescence signals were observed and recorded by a fluorescence microscope (Axiovert 200; Carl Zeiss; Göttingen, Germany) and a confocal microscope (LSM 780NLO; also from Carl Zeiss) [16].

2.10. FRET-based src biosensors

Cytosolic Src biosensor and the membrane-targeted Src biosensor, Lyn-Src biosensor, were previously described [30,31]. In brief, cytosolic Src biosensor is composed of a specific substrate for Src, a flexible linker, a SH2 domain between ECFP and YPet. Lyn-Src biosensor additionally contains membrane targeting signal derived from Lyn kinase in its *N*-terminal. In the default state of the biosensor, strong FRET is observed between ECFP and YPet. When activated Src phosphorylates the substrate in the biosensor, the phosphorylated substrate binds to the SH2 domain of the Src biosensor. This interaction induces the conformational changes of the biosensor, resulting in the decrease of FRET. Thus, by measuring the ECFP/FRET, we can visualize the activity of Src in live cells. In particular, membrane-targeted Src biosensor reports the local Src activity at plasma membrane, while cytosolic Src biosensor shows the overall Src activity throughout whole cell area.

2.11. Image acquisition of FRET

For the FRET imaging, cells were prepared on cover-glass-bottom dishes (SPL Life Sciences) coated with 10 μg/ml of fibronectin (Invitrogen). Images were collected by a Nikon Ti-E inverted microscope and a cooled charge-coupled device camera using NIS software with a 438DF24 excitation filter, a 458DRLP dichroic mirror, and two emission filters controlled by a filter changer (483DF32 for SECFP and 542DF27 for Venus). A neutral-density filter was used to control the intensity of the excitation light. The fluorescence intensity of non-transfected cells was quantified as the background signals and subtracted from the SECFP and Venus signals on transfected cells. The pixel-by-pixel ratio images of FRET/ECFP were calculated based on the background-subtracted fluorescence intensity images of ECFP and Venus by the NIS-Elements program (Nikon) to allow the quantification and statistical analysis of FRET responses. Red fluorescent images were collected using a 562DF40 excitation filter, a 593DRLP dichroic mirror, and a 641DF75 emission filter. Blue fluorescent images were acquired using a 377DF50 excitation filter, a 409 dichroic mirror, and a 447DF60 emission filter. Green fluorescent images and Venus images were collected using a 482DF35 excitation filter, a 506DRLP dichroic mirror, and a 536DF40 emission filter.

2.12. Chromatin immunoprecipitation (ChIP) and sequencing and PCR

We performed the ChIP using Abcam protocol (Abcam; Cambridge, UK). Briefly, the cells were stimulated with Wnt3A, then treated with formaldehyde (final concentration, 0.75%) for 15 min, and were subsequently disrupted with sonication in the ChIP lysis buffer (RIPA

buffer). The nuclei were harvested and then disrupted by sonication. *Anti-p*-Tyr42 Rho antibody was incubated with the DNA fragment-protein complex and precipitated by protein A-beads. The beads were then washed and the bound DNAs were eluted by the elution buffer (1% SDS and 100 mM $NaHCO_3$). RNA and proteins were removed by the incubation with RNAse and proteinase K. Finally, DNA was purified by phenol:chloroform extraction. The DNA fragments were used for sequencing and PCR with primers. DNA sequencing was performed in Ebiogen (Seoul, Korea) and PCR primers for *Vim* (mouse chromosome 2, 13574119–13574262: forward, 5′-ATTAGTAACAGGACTGTGCTTGTA-3'; reverse, 5′-AGGGTCCCCTCCCACT GCCATCTA-3′) were synthesized by Bioneer (Daejeon, Korea).

2.13. Analysis of survival probability of gastric cancer patients

We determined relative *p*-Tyr42 Rho levels in gastric cancer patient tissues and categorized them into two groups of low and high *p*-Tyr42 Rho expressers. The samples were obtained from the Cancer Centre of Busan National University Hospital (Busan, Korea), which is supported by the National Cancer Center of Korea. Information on death and survival of the patients were obtained from the Korean Statistical Information Service (KOSIS) of the Korean government and approved by the institutional review board (IRB) of Hallym University (Chuncheon, Korea).

2.14. Statistical analysis

All experiments were performed at least in triplicate, and intra-assay samples was analyzed in duplicate or triplicate. The data are presented as mean ± SE. Statistical comparison was made with Student's *t*-test using GraphPad Prism program (GraphPad Software, San Diego, USA) and differences between two groups were considered to be statistically significant if P values were less than the specified limit (*$P < 0.05$, **$P < 0.01$, ***$P < 0.001$).

3. Results

3.1. Wnt3A induces superoxide production through ROCK2 and p-p47phox

In this study, we found that Wnt3A induces superoxide production in a time-dependent manner (Fig. 1A). However, Tat-C3 Rho inhibitor and Y27632 ROCK inhibitor abolished the Wnt3A-mediated superoxide production, suggesting that Rho and ROCK regulate superoxide generation from Wnt3A (Fig. 1B). Contrary to the high levels of superoxide produced in HEK293T cells, Wnt3A barely produced superoxide in human dermal fibroblast (HDF), a model of an untransformed cell (Fig. 1C). Notably, LiCl prevented superoxide generation, suggesting that GSK-3β activated by Wnt3A is required for superoxide production, although *p*-Ser9 GSK-3β induced by Wnt3A has been well known to be an inactive form (Fig. 1D). Phosphorylation at Ser345 of p47phox, a component of NADPH oxidase was induced by Wnt3A, but Tat-C3 and Y27632 abolished this phosphorylation, suggesting that p47phox phosphorylation through RhoA and ROCK activation is critical for superoxide formation (Fig. 1E). To examine whether ROCK is able to directly phosphorylate p47phox, first we compared amino acid sequences of p47phox with other substrate proteins of ROCK including GSK-3β, myosin phosphatase subunit 1 (MYPT1). Interestingly, p47phox had amino acid similarity including Ser345 with GSK-3β and MYPT1 (Fig. 1F). In agreement with this observation, an active fragment of purified ROCK2 could phosphorylate p47phox *in vitro* (Fig. 1G). Of note, ROCK2 was immunoprecipitated favorably with p47phox, while ROCK1 was readily immunoprecipitated with GSK-3β, suggesting that ROCK1 preferentially binds to GSK-3β while ROCK2 preferentially binds to p47phox (Fig. 1H). In addition, DPI and apocynin, inhibitors of NADPH oxidase markedly prevented superoxide production by Wnt3A, suggesting that NADPH oxidase is engaged in regulation of Wnt3A-mediated superoxide production (Fig. 1I). Moreover, NAC, DPI and apocynin suppressed cell proliferation upon Wnt3A addition, suggesting that Wnt3A stimulates cell proliferation through at least in part ROS (Fig. 1J). Meanwhile, si-nucleoredoxin (si-NRX) significantly enhanced superoxide production in response to Wnt3A compared to control si-RNA, suggesting that NRX suppresses Wnt3A-mediated superoxide production (Fig. 1K).

3.2. Wnt3A increases p-Tyr42 RhoA and both p-Ser9 and p-Tyr216 GSK-3β levels

In a previous report, we found that Tyr42 phosphorylation of RhoA (*p*-Tyr42 RhoA) is induced by hydrogen peroxide (H_2O_2) in RAW264.7 cells, a macrophage cell line [18]. Here, hydrogen peroxide also induced Tyr42 phosphorylation of Rho GTPase in HEK293T cells (Fig. 2A). Consistent to the result of Fig. 1B, si-RhoA abolished superoxide production, and reconstituted RhoA WT and phospho-mimetic RhoA Y42E restored superoxide production. However, reconstituted dephospho-mimetic RhoA Y42F could not recover superoxide production in response to Wnt3A, suggesting that *p*-Tyr42 RhoA, in turn, regulates superoxide production (Fig. 2B). Wnt3A also elevated levels of β-catenin, *p*-Tyr416 Src (mouse; human in *p*-Tyr419), *p*-Ser9 GSK-3β and *p*-Tyr216 GSK-3β as well as *p*-Tyr42 Rho (Fig. 2C). ROS scavenger, NAC and NADPH oxidase inhibitors, DPI and apocynin abolished upregulation of *p*-Tyr42 Rho, β-catenin, *p*-Tyr416 Src, *p*-Ser9 GSK-3β and *p*-Tyr216 GSK-3β upon Wnt3A in HEK293T cells, suggesting that superoxide is closely involved in the increases of the above molecules via Wnt3A (Fig. 2C). PP2 Src inhibitor suppressed not only *p*-Tyr416 Src but also *p*-Tyr216 GSK-3β and p-Try42 Rho levels (Fig. 2D). Real time measurement of membranous and cytosolic Src activities revealed that membranous Src activity was reduced while cytosolic Src was activated in response to Wnt3A in 293 A cells (Fig. 2E). Likewise, a stimulant such as platelet-derived growth factor (PDGF) ensures Src translocation from the plasma membrane to the cytosol along with 4-fold activation of its kinase activity [32]. Since proline rich tyrosine kinase 2 (PYK2) activity was reported to be reduced by C3-transferase and Y27632 [33] and PYK2 can phosphorylate Tyr216 residue of GSK-3β [34,35], we examined PYK2 involvement in Wnt3A signaling in this study. PF431396, an inhibitor of PYK2 which is a member of Src family prevented *p*-Tyr216 GSK-3β, but not *p*-Ser9 GSK-3β, suggesting PYK2 regulates *p*-Tyr216 GSK-3β upon Wnt3A (Fig. 2F). In addition, si-Src inhibited *p*-Tyr216 GSK-3β, suggesting that Src is also directly participated in the Tyr216 phosphotylation of GSK-3β (Fig. 2G). Meanwhile, Y27632 inhibited both *p*-Tyr216 and *p*-Ser9 GSK-3β (Fig. 2H). As *p*-Ser9 and *p*-Tyr216 GSK-3β were known to be inactive and active forms of GSK-3β, respectively, we examined localization of *p*-Ser9 and *p*-Tyr216 GSK-3β in 293 A cells with a feature of flattened large shape. There were three pools of GSK-3β such as *p*-Ser9 (green color), *p*-Tyr216 (red color) and co-localized GSK-3β (yellow color) in 293 A cells. However, Wnt3A enhanced the intensity of *p*-Tyr216 GSK-3β, which was also enriched in peripheral region including plasma membrane, whereas *p*-Ser9 GSK-3β was localized mainly in cytosol region (Fig. 2I). ROCK1 was co-immunoprecipitated preferentially with RhoA, but much less with *p*-Tyr42 RhoA. However, ROCK2 was preferentially co-immunoprecipitated with *p*-Tyr42 RhoA upon Wnt3A, although ROCK2 was co-immunoprecipitated less with RhoA. The results suggest that ROCK2 is a preferential downstream effector protein of *p*-Tyr42 RhoA while ROCK1 is activated dominantly by RhoA (Fig. 2J). Furthermore, ROCK2 preferentially associates with p-p47phox (Fig. 1H), suggesting that *p*-Tyr42 RhoA/ROCK2/p-47phox signaling pathway may contribute superoxide production upon Wnt3A stimulation.

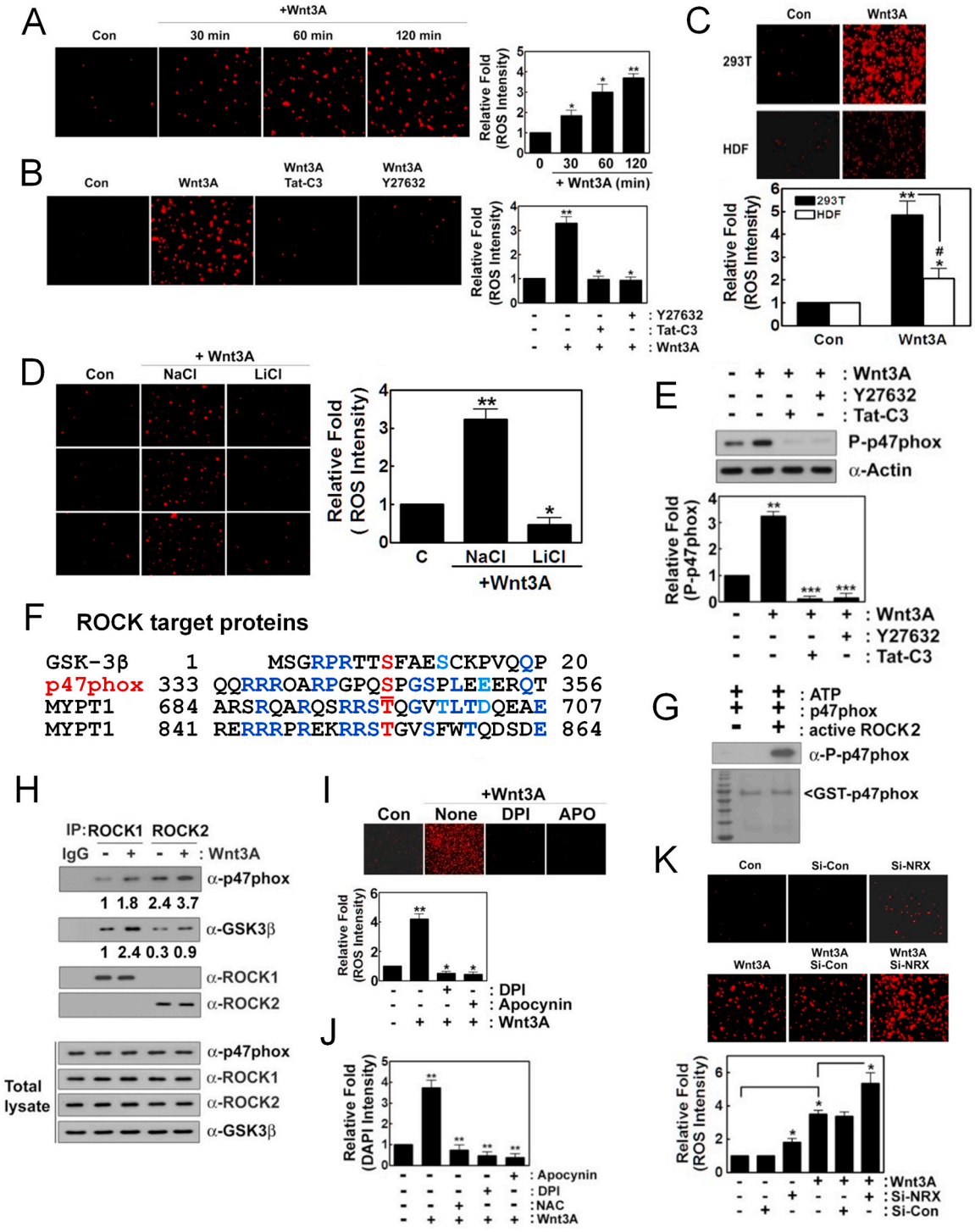

Fig. 1. Wnt3A induces superoxide production through ROCK2 and p47phox. (A) HEK293T cells (2–5x10^4) were cultured in DMEM 5% FBS and 1% P/S. For Wnt3A signaling, they were starved for 12 h without serum and treated with Wnt3A (30 ng/ml) for the indicated periods. Produced superoxide was visualized with hydroethidine (1 μM) for 5–15 min, detected using a fluorescence microscope (Axiovert 200, Carl Zeiss). (B) Cells were pretreated with Tat-C3 (0.1 μg/ml) and Y27632 (10 μM) for 1 h and then activated with Wnt3A (30 ng/ml) for 2 h and superoxide was detected with hydroethidine as in (A). (C) Human dermal fibroblast (HDF) and HEK293T cells (2–5x10^4) were treated with Wnt3A (30 ng/ml) for 2 h and the produced superoxide was detected as in (A). (D) Cells were pretreated with LiCl (20 mM) or NaCl (20 mM) for 1 h and then treated with Wnt3A (30 ng/ml) for 2 h with produced superoxide detected as above. (E) Cells were pretreated with Tat-C3 (0.1 μg/ml), Y27632 (10 μM) for 1 h and then treated with Wnt3A (30 ng/ml) for 2 h. *P*-Ser345 p47phox level changes were determined with western blotting. (F) Amino acid sequences of GSK-3β, p47phox, myosin phosphatase 1 (MYPT1) were compared. (G) Recombinant purified GST-p47phox (0.2 μg) protein was incubated with an active fragment of purified ROCK2 protein (0.1 μg), ATP (0.1 mM) and $MgCl_2$ (1 mM) for 30 min at RT. *P*-Ser345 p47phox was detected by western blotting. (H) HEK293T cells were stimulated with Wnt3A and ROCK1 and ROCK2 were immunoprecipitated and co-precipitated p-47phox and GSK-3β were determined by western blotting. (I, J) Cells were pretreated with DPI (10 μM) and apocynin (10 μM) for 1 h and then treated with Wnt3A (30 ng/ml) for 2 h and produced superoxide was detected as above (I), and cell proliferation was determined using DAPI staining (J). (K) HEK293T cells were transfected with si-control and si-nucleoredoxin (NRX) (10 nM) for 72 h, then treated with Wnt3A (30 ng/ml) for 2 h with the produced superoxide detected as described above.

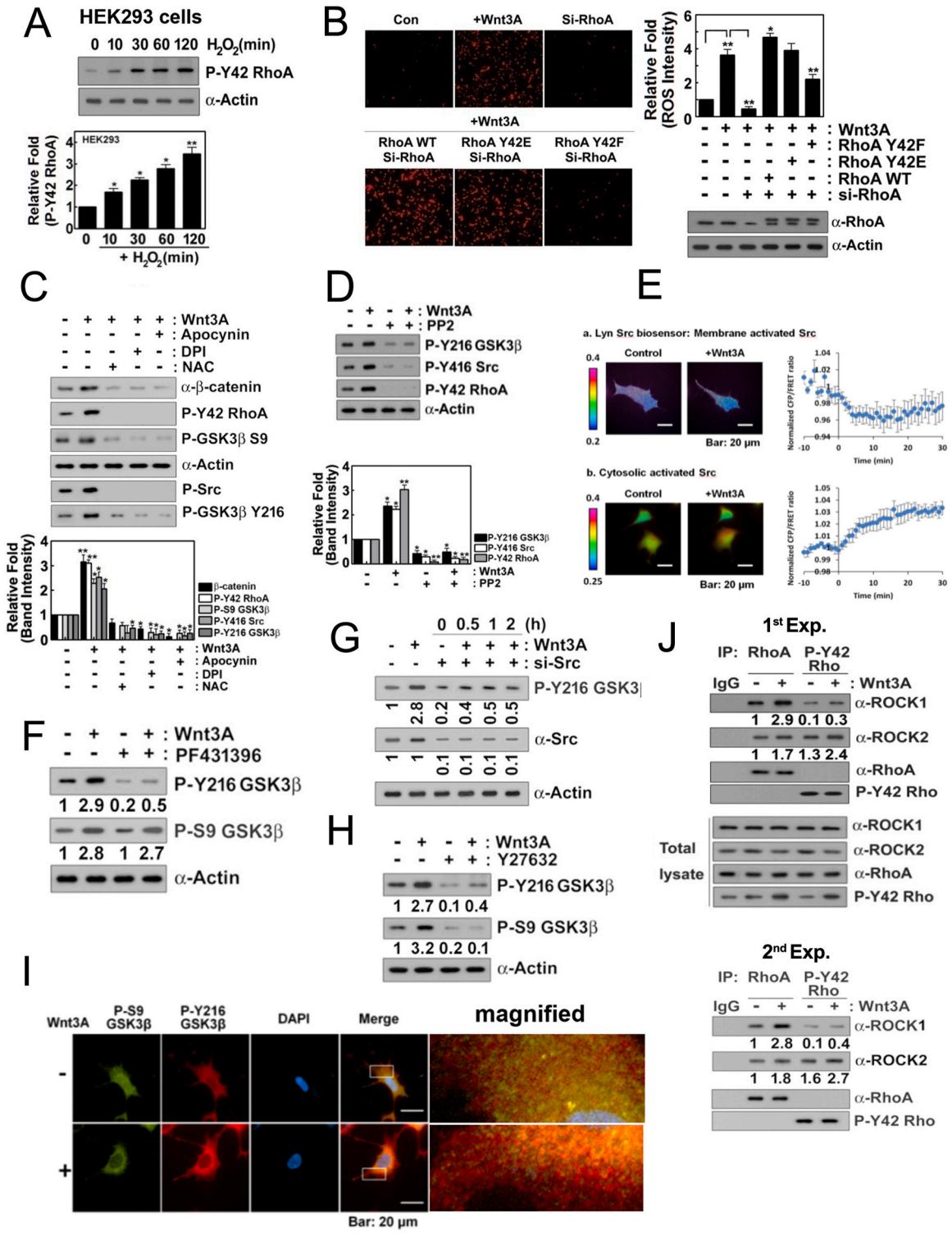

Fig. 2. Wnt3A increases *p*-Tyr42 RhoA and both *p*-Ser9 and *p*-Tyr216 GSK-3β levels. (A) HEK293T cells (2–5x10^5) were treated with H_2O_2 (100 μM) for the indicated periods and *p*-Tyr42 RhoA was detected by western blotting. (B) HEK293T cells were transfected with si-RhoA (10 nM) for 72 h and then transfected with RhoA WT, Y42E and Y42F plasmid DNA (4 μg) for 18 h. Produced superoxide was detected with hydroethidine as above. (C) Cells were pretreated for 1 h with NAC (10 mM), DPI (10 μM), and apocynin (10 μM) and the indicated proteins were detected by western blotting. (D) Cells were pretreated with PP2 (10 μM) for 1 h and then treated with Wnt3A (30 ng/ml) for 2 h and subsequently, the indicated proteins were detected by western blotting. (E) Real time activation of Src in membrane and cytosol of 293 A cells was measured using FRET methods. (F) HEK293T cells were pretreated with PF431396 (10 μM), an inhibitor of PYK2, stimulated by Wnt3A and then *p*-Tyr216 and *p*-Ser9 GSK-3β were determined. (G) Cells were transfected with si-Src and stimulated by Wnt3A. *p*-Tyr216 GSK-3β was determined by immunoblotting. (H) HEK293T cells were pretreated with Y27632 (10 μM) for 1 h and then treated with Wnt3A (30 ng/ml) for 2 h; *p*-Tyr216 GSK-3β level changes were detected by western blotting. (I) 293 A cells were incubated for 12 h without serum and were then treated with Wnt3A (50 ng/ml) for 30 min. Cells were then fixed using 4% PFA and *p*-Ser9 GSK-3β (green: Alexa-488) and *p*-Tyr216 GSK-3β (red: Alexa546) levels were visualized with the respective secondary antibodies. (J) Cells were stimulated with Wnt3A (30 ng/ml) for 2 h, RhoA and *p*-Tyr42 RhoA were immunoprecipitated and co-immunoprecipitated ROCK1 and ROCK2 were detected with western blotting. (For interpretation of the references to color in this figure legend, the reader is referred to the Web version of this article.)

3.3. p-Tyr216 and p-Ser9 GSK-3β temporally regualte β-catenin accumulation during the Wnt3A stimulation: p-Ser9 GSK-3β phosphorylates Ser493, Ser51 and Ser43 of src

We corroborated the observation that Wnt3A regulates levels of β-catenin, *p*-Tyr416 Src, *p*-Tyr216 GSK-3β and *p*-Tyr42 RhoA in a time-dependent manner, with a steady increase in activity up to 120 min post treatment and then followed by a decline. However, for *p*-Ser9 GSK-3β levels, they begin to increase after 120 min post treatment with Wnt3A (Fig. 3A). In addition, RhoA-GTP maximal levels are achieved between 60 and 120 min following treatment with Wnt3A (Fig. 3B). Herein, we explored whether *p*-Ser9 or *p*-Tyr216 GSK-3β regulated β-catenin accumulation in a series of experiments with various recombinant mutants of GSK-3β. In vitro, either the phospho-mimetic GSK-3β Y216E or the dephospho-mimetic GSK-3β S9A elevated the levels of β-catenin, *p*-Tyr416 Src and *p*-Tyr42 RhoA. On the other hand, neither dephospho-mimetic GSK-3β Y216F nor phospho-mimetic GSK-3β S9D could do the same (Fig. 3C and sFig. 1A). These results suggest that upon Wnt3A stimulation, *p*-Tyr216 GSK-3β and dephospho-Ser9 GSK-3β, both of which are known to be active forms of GSK-3β, are critical for β-catenin accumulation along with Tyr416 phosphorylation of Src and Tyr42 phosphorylation of RhoA (Fig. 3C). In the same experiments, GSK-3β Y216F abolished *p*-Ser1490 LRP6, suggesting that *p*-Tyr216 GSK-3β was critical for Ser1490 phosphorylation of LRP6 upon Wnt3A treatment of the cells (Fig. 3C).

To delineate how GSK-3β potentially regulates Src activity, we performed a series of experiments with a number of *in vitro* kinase assays using Src and mutants of GSK-3β in presence of ATP/Mg^{2+}. The inactive mimetic forms of GSK-3β S9D or Y216F but neither the active mimetic forms GSK-3β S9A nor Y216E markedly reduced *p*-Tyr416 Src levels. Interestingly, GSK-3β S9D, known to be a phospho-mimic inactive kinase form of the enzyme, apparently could also increase Ser phosphorylation of Src *in vitro* (Fig. 3D and sFig. 1B). This suggested that S9D and Y216F GSK-3β modulated Src activity. In Wnt3A-treated cells, Wnt3A augmented Ser phosphorylation of Src (Fig. 3E). Src was also already associated with GSK-3β and *p*-Ser9 GSK-3β before and after Wnt3A activation of the cells as demonstrated by co-immunoprecipitation (Fig. 3E). These findings suggested that Src was a potential substrate of *p*-Ser9 GSK-3β, it being able to phosphorylate Src in vivo.

We next studied the amino acid sequence of Src in comparison to those of β-catenin and glycogen synthase (GS) for putative Ser phosphorylation site(s) of Src by GSK-3β. β-Catenin and GS are both already known to be substrates of GSK-3β. Src had a high degree of amino acid sequence similarity with GS in various regional domains, and we hypothesized that Ser493 (human; Ser490 in chicken) (sFig. 1C) residue of SH1 domain might be a candidate for phosphorylation by *p*-Ser9 GSK-3β (Fig. 3F). Ser35, Ser39, Ser43 and Ser51 of Src Unique domain were also analogous to Ser33, Ser37, Ser41 and Ser49 of β-catenin, all in domains harboring high levels of proline residues, similar to GS. Among them, Ser41, Ser37 and Ser33 residues are known to be potential GSK-3β phosphorylation sites (Fig. 3F). We determined the phosphorylation sites of Src by GSK-3β *in vitro* by kinase assays set up with recombinant GST-S9D GSK-3β and Src protein in presence of ATP/$MgCl_2$. The kinase products were analyzed by MALDI-TOF. Consequently, Ser51 of Src was determined to be tentatively phosphorylated by GSK-3β (Fig. 3G) with partial homology to the corresponding Ser residue in β-catenin and GS (Fig. 3F). Positions of *p*-Ser candidate residues in several domains of Src were shown (Fig. 3H).

To verify that various Ser residues of Src can become phosphorylated post treatment with Wnt3A, we prepared mutants of Src including versions D5 (S493D/S51D/S43D/S39D/S35D), D4 (S493D/S51D/S43D/S39D), D3 (S493D/S51D/S43D), and D2 (S493D/S51D). The D5, D4, and D3 Src versions had no *p*-Ser signals detected, while the D2 version had a *p*-Ser signal upon Wnt3A treatment, indicating that S43 of Src was can be phosphorylated in response to Wnt3A (sFig. 2A). To confirm this separately, we explored the Ser phosphorylation signals with S493A, S51A, and S43A mutants of Src. In particular, S493A and S51A had low *p*-Ser Src signals and had higher *p*-Tyr416 Src levels, while S43A had high *p*-Ser Src signals and low *p*-Tyr416 Src levels (Fig. 3I). On the other hand, S493D and S51D had increased *p*-Ser Src signals along with reduced *p*-Tyr416 Src signals, while S43D had reduced *p*-Ser Src signals along with increased signals for *p*-Tyr416 Src (Fig. 3J and sFig. 2B).

Moreover, both Src versions, D3 (S493D/S51D/S43D), A3 (S493A/S51A/S43A), and A2 (S493A/S51A) had abolished *p*-Ser Src signals along with high *p*-Tyr416 Src levels and the association with ROCK2 (Fig. 3K and sFig. 2C-2E). As both S43A/S493A and S43A/S51A Src mutants were Ser-phosphorylated post Wnt3A treatment, this suggested that Ser51 and Ser493 of Src were the phosphorylation sites in Src following the cell activation by Wnt3A (sFig. 2E).

Moreover, *p*-Tyr216 GSK-3β, *p*-Tyr42 RhoA and ROCK2, but neither p-S9 GSK-3β nor ROCK1 were associated with Src S493A, S51A, S43D, S51A/S493A (A2), S43/51/493D (D3) and S43/51/493 A (A3) (Figs. 3I-3K and sFig. 2B). In addition, *p*-Ser9 GSK-3β/ROCK1 and *p*-Tyr216 GSK-3β/ROCK2/p-Tyr42 RhoA were reciprocally associated with Src, depending on the phosphorylation states of Src, as revealed by *p*-Ser and *p*-Tyr416 levels of Src (Fig. 3I-Figs. 3I-3K). GSK-3β S9A could not phosphorylate Src Ser residues upon Wnt3A treatment, suggesting that *p*-Ser9 GSK-3β was a valid kinase in phosphorylating Ser residues of Src in response to Wnt3A stimulation (Fig. 3L). From these results, depicted in a schematic, we propose Ser493 and Ser51 phosphorylation of Src by *p*-Ser9 GSK-3β, leading to Src inactivation and subsequent phosphorylation of Src Ser43, recovering the Src activity (Fig. 3M).

3.4. Wnt3A induces formation of RhoA/β-catenin complex

Remarkably, we observed that β-catenin was co-immunoprecipitated with RhoA upon Wnt3A (Fig. 4A). In turn, *p*-Tyr42 Rho was also co-immunoprecipitated with β-catenin (Fig. 4B). As lysophosphatidic acid (LPA) has been reported to activate β-catenin along with nuclear translocation of β-catenin [36,37], the possibility of formation of a complex of β-catenin/RhoA or *p*-Tyr42 Rho by LPA was explored. LPA did not change the levels of RhoA and β-catenin, while *p*-Tyr42 Rho levels were apparently increased (Fig. 4C). Likewise, co-immunoprecipitation of RhoA and β-catenin was clearly observed, but the relative levels of the co-immunoprecipitants were rarely altered. Association of β-catenin and *p*-Tyr42 Rho shown via co-immunoprecipitation, however, was notably increased with LPA treatment (Fig. 4C). We next tried to identify whether GDP/GTP-bound states of RhoA determine the interaction between RhoA and β-catenin. Recombinant GST-β-catenin binding to RhoA-GTPγS or RhoA-GDP *in vitro* was not significantly different, suggesting that GDP or GTP binding to RhoA is not critical for regulating interaction between RhoA with β-catenin (Fig. 4D).

To identify the specific domain of β-catenin associating with RhoA, we expressed and purified GST-fusions of β-catenin domains composed of amino acids (aa) 1–140, 141–390, 391–662 and 663–782 (Fig. 4E and F). Of note, three dimensional (3D) structure of β-catenin armadillo repeat (ARM) domain was presented. However, *N*-terminal domain (NTD) of β-catenin was only partially revealed in Lys21-Pro44 and Asp83-Ile140 peptide fragments, whereas other parts of the NTD were not determined (http://www.sbg.bio.ic.ac.uk/phyre2/html/page.cgi?id=index; http://proteopedia.org). RhoA preloaded with GTPγS readily bound to aa 1–140 NTD of GST-β-catenin domain, conjugated to beads, whereas other domain fusion proteins only marginally bound to RhoA (Fig. 4G). Also, only the ectopic expression of NTD (aa 1–140) markedly interfered with cell proliferation due to Wnt3A (Fig. 4H).

3.5. Tyr42 phosphorylation of RhoA is critical for binding to β-catenin

We next examined whether *p*-Tyr42 RhoA regulates β-catenin level. Remarkably, si-RhoA impaired β-catenin accumulation, but re-constitutive dephospho-mimetic RhoA Y42F as well as RhoA WT and

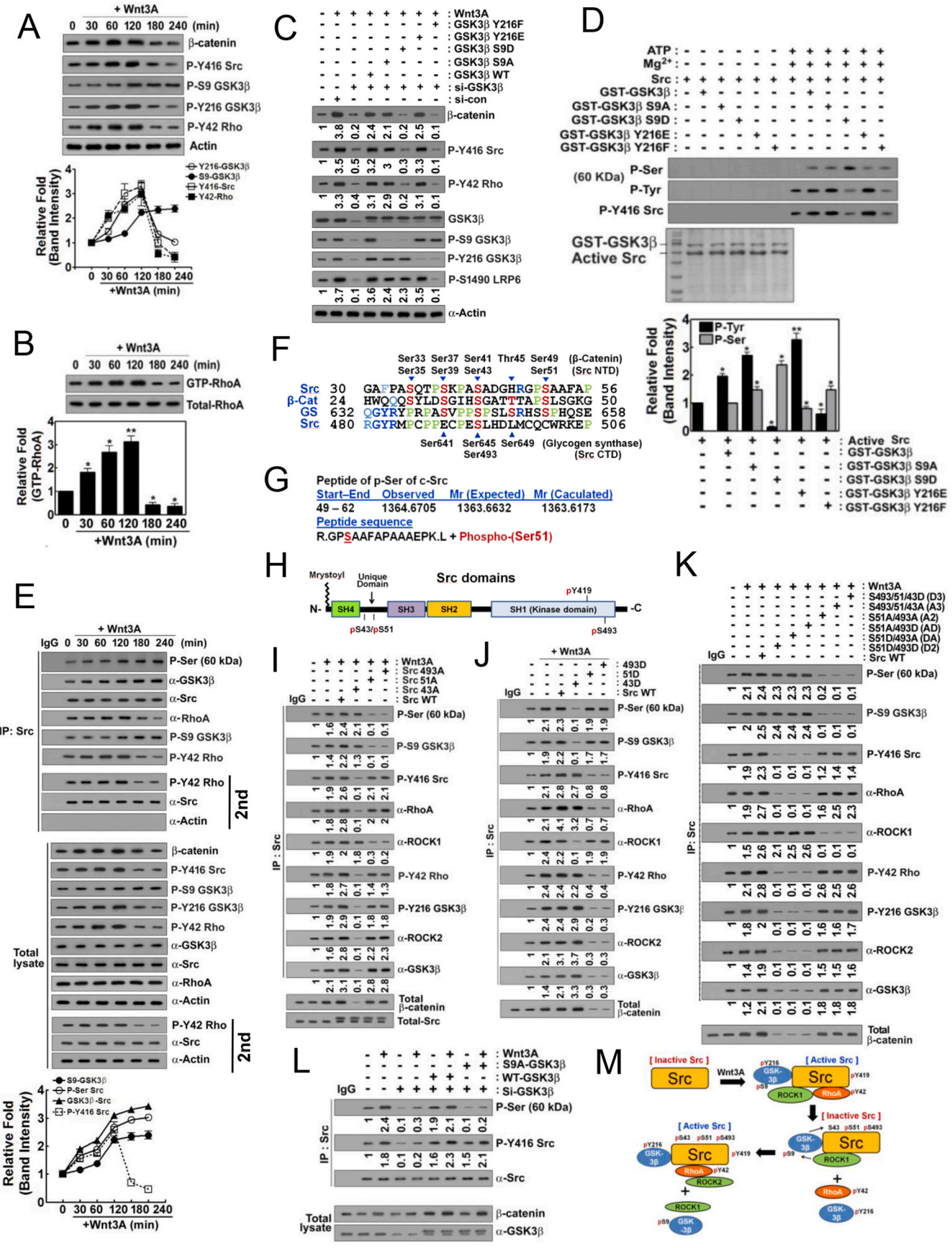

(caption on next page)

Fig. 3. *P*-Tyr216 GSK-3β stimulates β-catenin in early period and then *p*-Ser9 GSK-3β attenuates β-catenin through Src phosphorylation in late period of Wnt3A stimulation. (A) HEK293T cells were stimulated by Wnt3A in time-dependent manner and indicated proteins were determined. (B) RhoA-GTP levels were determined using RBD-beads pull-down assay. (C) HEK293T cells were transfected with si-GSK3β and reconstituted with GSK-3β WT, S9A, S9D, Y216E and Y216F. Cells were stimulated by Wnt3A (30 ng/ml) for 2 h and indicated proteins were determined. (D) Recombinant GST-GSK-3β WT, S9A, S9D, Y216E and Y216F proteins were incubated with Src protein in the presence of ATP (20 μM) and $MgCl_2$ (25 mM) for 60 min and *p*-Ser and *p*-Tyr416 Src were detected with western blotting. (E) HEK293T cells were stimulated with Wnt3A (30 ng/ml) for 2 h and Src was immunoprecipitated and then indicated proteins were detected. (F) Amino acids sequences of *N*- (NTD) and *C*-terminal domains (CTD) of Src, β-catenin and glycogen synthase (GS) were compared. Identical amino acids were indicated in blue and similar ones were noted in cyan blue. Specific Ser candidate residues to be phosphorylated were noted in red. Particularly identical proline residues were noted in green. (G) GST-GSK-3β S9D and Src proteins were incubated with ATP/$MgCl_2$, the SDS-PAGE was performed, and Src protein was analyzed to identify phosphorylation site by using MALDI-TOF. Ser51 was identified to be phosphorylation site. (H) Domains of Src including SH4, Unique domain (UD), SH3, SH2, and SH1 was presented. *P*-Ser51 and *p*-Ser43 were localized in UD and *p*-Ser493 was localized in SH1 domain. (I) Cells were transfected with Src S493A, S51A, S43A mutants and WT (wild type), then Src was immunoprecipitated and then *p*-Ser and *p*-Tyr416 Src, p-S9 GSK-3β, *p*-Tyr216 GSK-3β, *p*-Tyr42 RhoA, ROCK1, and ROCK2 were immunoblotted. (J) Cells were transfected with Src S493D, S51D, S43D mutants, and WT (wild type), then Src was immunoprecipitated and then *p*-Ser and *p*-Tyr416 Src, p-S9 GSK-3β, *p*-Tyr216 GSK-3β, *p*-Tyr42 RhoA, ROCK1 and ROCK2 were immunoblotted. (K) Cells were transfected with Src A3 (S493A/S51A/S43A), D3 (S493D/S51D/S43D), A2 (AA: S493A/S51A), D2 (DD: S493D/S51D), AD (S493A/S51D) and DA (S493A/S51A), and WT (wild type) and Sc was immunoprecipitated and then *p*-Ser and *p*-Tyr416 Src, p-S9 GSK-3β, *p*-Tyr216 GSK-3β, *p*-Tyr42 RhoA, ROCK1 and ROCK2 were immunoblotted. (L) si-GSK-3β, GSK-3β WT and GSK-3β S9A were transfected and treated with Wnt3A for 2 h. Src was immunoprecipitated and *p*-Ser was immunoblotted. (M) Tentative model for *p*-Ser9 GSK-3β to phosphorylate Ser493, Ser51, and Ser43 residues of Src was presented. *p*-Ser493 and *p*-Ser51 Src are inactive forms, but *p*-Ser43 Src is an active form. (For interpretation of the references to color in this figure legend, the reader is referred to the Web version of this article.)

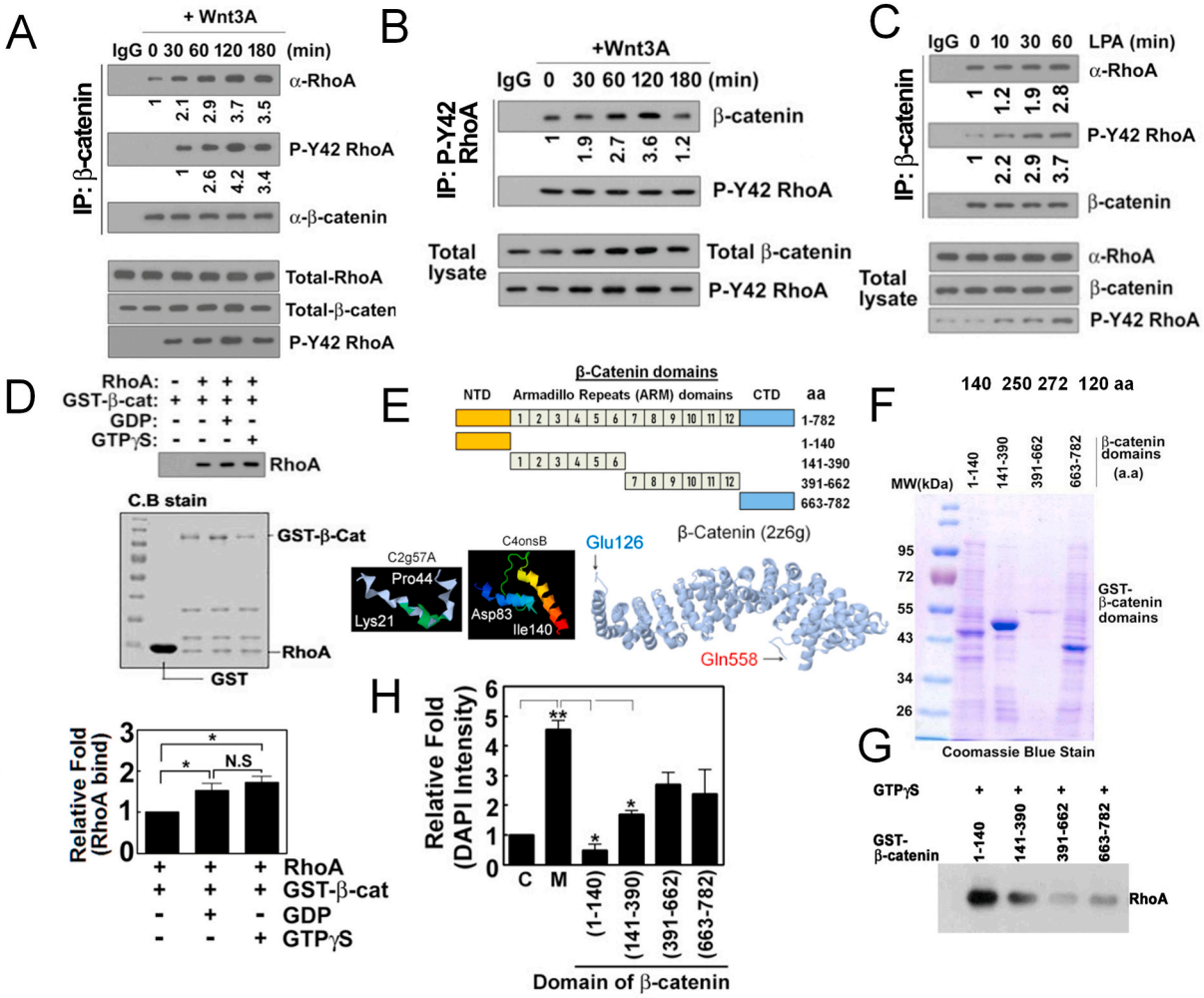

Fig. 4. β-Catenin interacts with *p*-Tyr42 RhoA in response to Wnt3A. (A, B) HEK293T cells (2–5x10^5) were stimulated with Wnt3A (30 ng/ml), β-catenin and *p*-Tyr42 Rho were immunoprecipitated from cell lysates and co-immunoprecipitated RhoA and β-catenin were detected by western blotting (A and B, respectively). (C) LPA (10 μM) was treated to HEK293T cells and β-catenin was immunoprecipitated from cell lysates and co-immunoprecipitated RhoA and *p*-Tyr42 RhoA were detected by western blotting. (D) Recombinant purified RhoA (0.1 μg/50 μl) was preloaded with GDP or GTPγS for 30 min and then was incubated with GST-β-catenin (0.1 μg/50 μl) for 2 h. RhoA associated with GST-β-catenin was detected by western blotting. (E) Schematic of the domains and partial 3D structure of β-catenin are shown. (F) Recombinant purified domains of β-catenin were run with SDS-PAGE and stained with Coomassie-blue. (G) RhoA associated with several domains of GST-β-catenin was detected by western blotting. (H) Cells were transfected with plasmid DNAs of various domains of β-catenin and cell proliferation stimulated by Wnt3A (30 ng/ml) was assayed by DAPI staining. (For interpretation of the references to color in this figure legend, the reader is referred to the Web version of this article.)

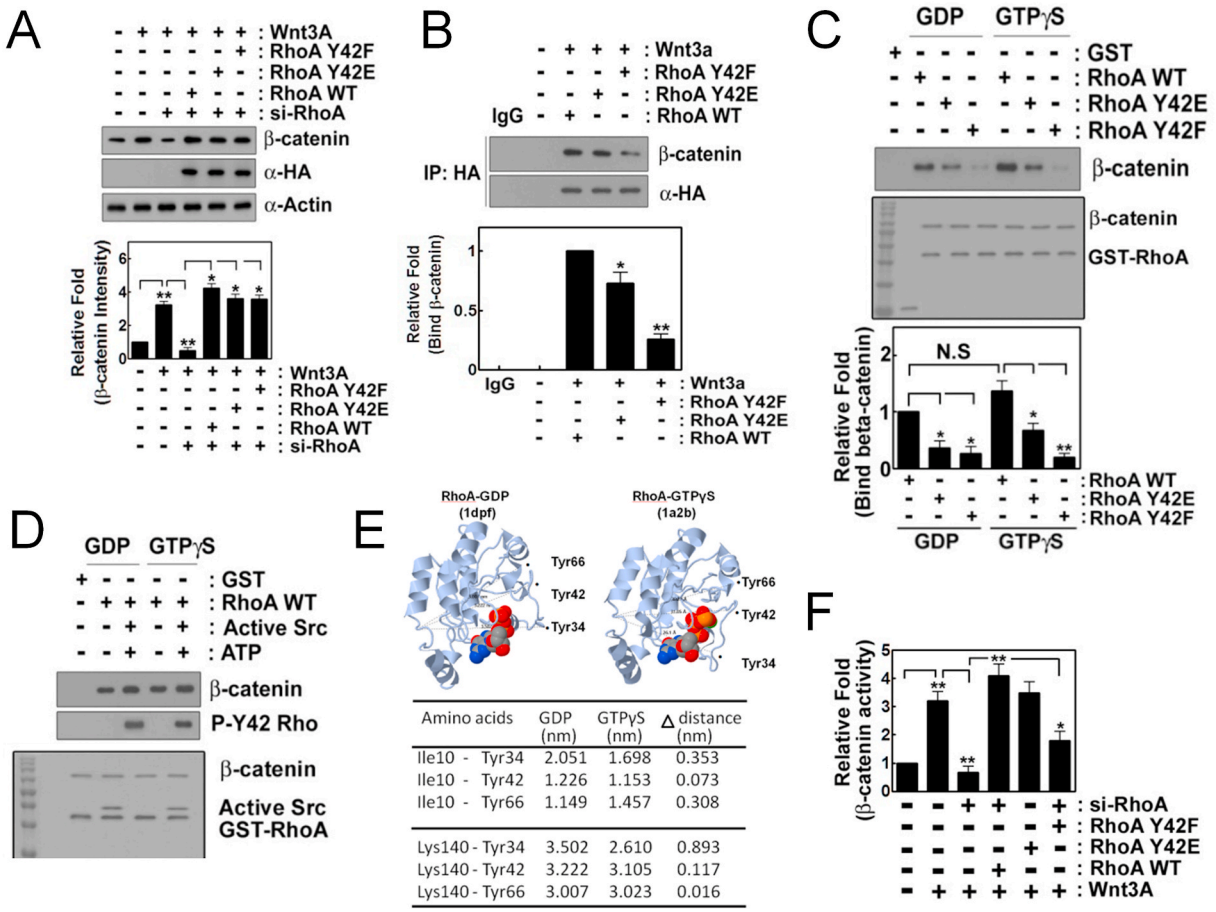

Amino acids	GDP (nm)	GTPγS (nm)	Δ distance (nm)
Ile10 - Tyr34	2.051	1.698	0.353
Ile10 - Tyr42	1.226	1.153	0.073
Ile10 - Tyr66	1.149	1.457	0.308
Lys140 - Tyr34	3.502	2.610	0.893
Lys140 - Tyr42	3.222	3.105	0.117
Lys140 - Tyr66	3.007	3.023	0.016

Fig. 5. *P*-Tyr42 RhoA interacts with β-catenin. (A) HEK293T cells (2–5x10^5) were transfected with si-RhoA (10 nM) for 72 h and were then transfected with HA-RhoA WT, Y42E and Y42F (4 μg plasmid DNA) for 24 h. Cells were treated with Wnt3A (30 ng/ml) for 2 h and β-catenin was detected by western blotting. (B) HA-containing RhoA was immunoprecipitated and β-catenin co-immunoprecipitated with RhoA was detected with western blotting. (C) Recombinant purified GST-RhoA (0.1 μg/50 μl) that was preloaded with GDP or GTPγS was incubated with β-catenin (0.1 μg/50 μl) for 30 min at RT *in vitro*. β-Catenin associated with GST-RhoA was detected with western blotting. (D) Recombinant purified GSH beads-GST-RhoA (0.1 μg/50 μl) that was preloaded with GDP or GTPγS was incubated with purified Src (0.1 μg/50 μl), ATP (20 μM) and $MgCl_2$ (25 mM) for 30 min to phosphorylate Tyr42 of RhoA and then β-catenin (0.1 μg/50 μl) was added and incubated more for 1 h. β-Catenin associated with GSH beads-GST-RhoA was detected with western blotting. (E) Three dimensional structures of RhoA-GDP and -GTPγS and Tyr34, Tyr42 and Tyr66 were indicated. Distances from Ile10 or Lys140 to Tyr34, Tyr42 and Tyr66 of RhoA in the presence of GDP or GTPγS were measured using Proteopia site. (F) HEK293T cells were transfected with si-RhoA for 72 h, then with RhoA WT, Y42E and Y42F along with β-catenin promoter-luciferase DNA (2 μg) for 24 h and luciferase activity was measured.

phospho-mimetic RhoA Y42E allowed recovery of β-catenin accumulation (Fig. 5A). This result suggests that RhoA is critical for β-catenin accumulation with Wnt3A stimulation, but that *p*-Tyr42 of RhoA is not essential for β-catenin accumulation. We then examined whether *p*-Tyr42 residue of RhoA is critically involved in interaction with β-catenin. β-Catenin was co-immunoprecipitated with WT RhoA and RhoA Y42E, but much less with RhoA Y42F (Fig. 5B). GST-RhoA WT, Y42E and Y42F preloaded with GDP or GTPγS were incubated recombinant purified β-catenin *in vitro*. RhoA WT, but either RhoA Y42E or Y42F mutants was much less associated with β-catenin irrespective of GDP and GTP GTPγS (Fig. 5C). Similarly, GST-RhoA phosphorylated by Src and ATP [18] also readily bound to β-catenin *in vitro*, irrespective of GDP- or GTPγS-preloaded RhoA, suggesting that phosphorylation of Tyr42, but not GTP/GDP-binding state is critical for interaction between RhoA and β-catenin (Fig. 5D). Herein, we presented and compared 3D structure of RhoA-GDP [38] and -GTPγS [39] by using Proteopedia site (http://proteopedia.org/wiki/index.php/). Distances between Tyr34, Tyr42 and Tyr66 and Ile10 and Lys140, arbitrary standards in *N*- and *C*-terminal domains in GDP and GTPγS bound states of RhoA were calculated (Fig. 5E). Tyr34 and Tyr66 of RhoA are known to be also phosphorylated [40]. The 3D of RhoA revealed Tyr42 residue positioning in extended β2 region did not dramatically alter 3D location, while Tyr34 in switch 1 (aa 28–38) and Tyr66 in switch 2 (aa 61–78) regions revealed significant alteration [39] (Fig. 5E), suggesting that GDP or GTP may not contribute *p*-Tyr42 RhoA binding to β-catenin. Next, the effect of mutation of Tyr42 in RhoA on β-catenin activity in nucleus was assessed with RhoA Y42E and Y42F transfection in HEK293T cells. RhoA Y42F also had impaired luciferase activity for gauging β-catenin activity. Likewise, si-RhoA also prevented β-catenin activity, and reconstitution of RhoA WT and phospho-mimetic Y42E restored the β-catenin activity, but not with dephospho-mimetic RhoA Y42F, it having a remarkably reduced β-catenin activity (Fig. 5F).

3.6. *p-Tyr42 RhoA is critical for cell proliferation upon Wnt3A*

Wnt3A enhanced proliferation of HEK293T cells (Fig. 6A). However, RhoA inhibitor (Tat-C3) and ROCK inhibitor (Y27632) abolished this proliferation (Fig. 6B). Similarly, Tat-C3 and Y27632 also inhibited Wnt3A-mediated proliferation in the macrophage cell line RAW264.7 (Fig. 6C). RhoA Y42F transfection also markedly abrogated cell proliferation (Fig. 6D), consistent with β-catenin activity being due to the role of a phosphorylated Tyr42 in RhoA (Fig. 5F). Wnt3A also induced expression of cyclin D1 and *c*-Myc in the test cells, but Tat-C3 and Y27632 abolished this Wnt3A increased expression (Fig. 6E). RhoA WT

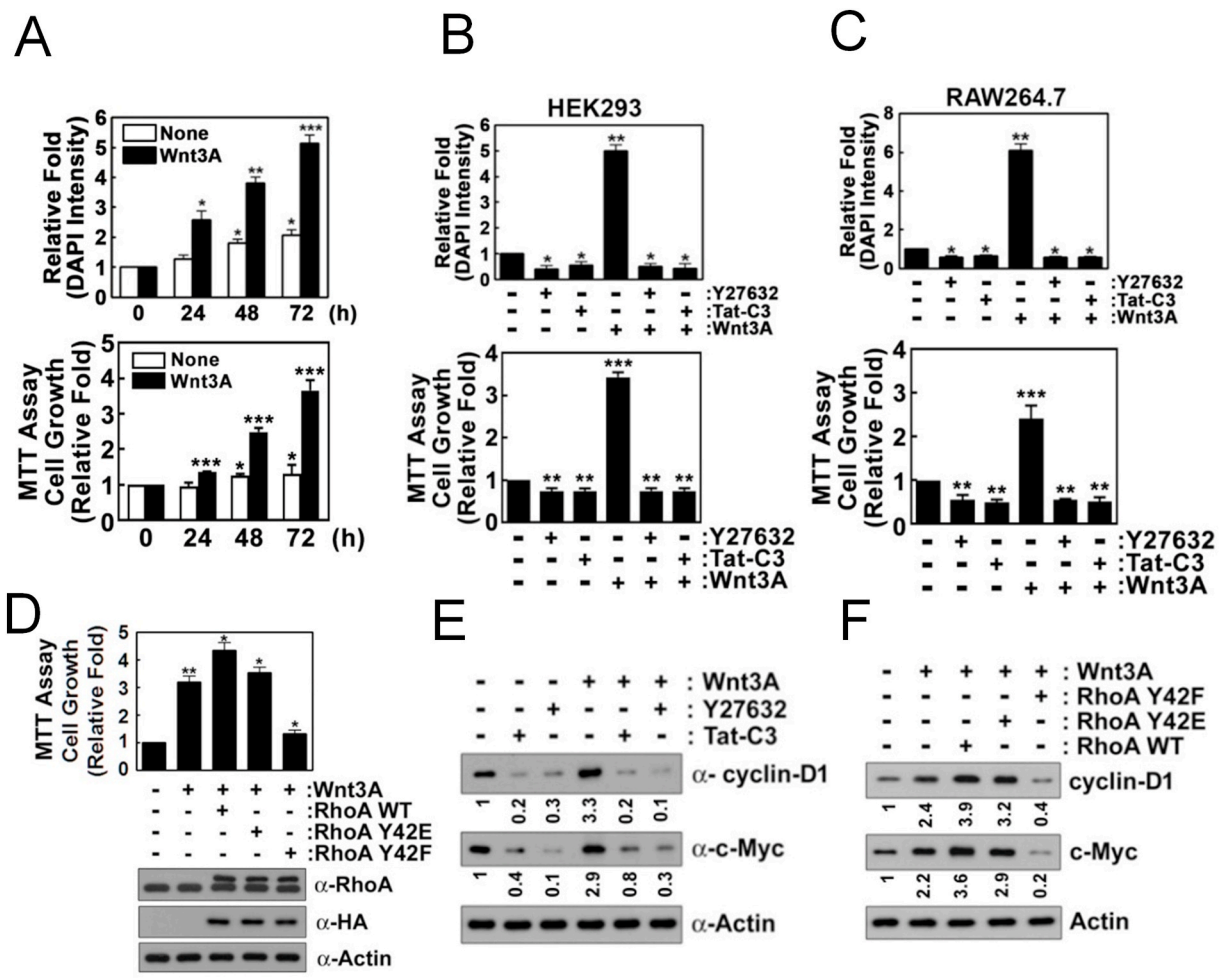

Fig. 6. *P*-Tyr42 RhoA induces cell proliferation in response to Wnt3A. (A) HEK293T cells were stimulated Wnt3A (30 ng/ml) for 48 h. Cell were stained with DAPI (1 μg/ml) for 10 min, and DAPI fluorescence was measured with a fluorescence microscope. In addition, cell proliferation was also measured using MTT assay. (B, C) HEK293T and RAW264.7 cells, respectively, were pretreated with Tat-C3 (1 μg/ml) and Y27632 (10 μM) for 1 h and then treated with Wnt3A (30 ng/ml) for 2 days. Cell proliferation was measured by measuring DAPI fluorescence with a fluorescence microscope. In addition, cell proliferation was also measured using MTT assay. (D) HEK293T cells were transfected with RhoA WT, Y42E and Y42F (4 μg DNA) for 24 h, then treated with Wnt3A (30 ng/ml) for 2 days. MTT assay was used for cell proliferation. (E) HEK293T cells were pretreated with Tat-C3 (1 μg/ml) and Y27632 (10 μM) for 1 h and then treated with Wnt3A (30 ng/ml) for 2 h and cyclin D1 and *c*-Myc were detected by western blotting. (F) HEK293T cells were transfected with RhoA WT, Y42E and Y42F (4 μg DNA) for 24 h, then treated with Wnt3A (30 ng/ml) for 2 days and cyclin D1 and *c*-Myc were detected by western blotting.

and RhoA Y42E transfection to cells also had increased expression of cyclin D1 and *c*-Myc in presence of Wnt3A, whereas RhoA Y42F transfection inhibited this cyclin D1 and *c*-Myc up-regulation (Fig. 6F).

3.7. Upon Wnt3A stimulation, p-Y42 RhoA is localized in the nucleus

Next, we explored the localization of RhoA/β-catenin complex. Wnt3A induced nuclear localization of β-catenin (Fig. 7A). However, si-RhoA interfered with β-catenin nuclear localization likely due to failure of β-catenin accumulation (Figs. 7A and 5F). We then followed any localization changes for RhoA and *p*-Tyr42 Rho with Wnt3A stimulation. Wnt3A did not affect the un-phosphorylated RhoA distribution compared with the control cells (Fig. 7B). However, *p*-Tyr42 Rho readily moved to the nucleus in response to Wnt3A (Fig. 7B). In addition, *p*-Tyr42 Rho localized in nuclear fraction was found to be increased whereas a decrease of *p*-Tyr42 Rho in cytoplasmic fraction was revealed when it was detected with Western blot (Fig. 7C). si-β-Catenin did not alter the nuclear localization of *p*-Tyr42 Rho (Fig. 7D and sFig. 3AFig. S3A. However, RhoA Y42F (dephospho-mimic) transfection remarkably interfered with nuclear localization of β-catenin due to Wnt3A (Fig. 7E and sFig. 3B), suggesting that Tyr42 phosphorylation of RhoA is critical for nuclear translocation of β-catenin. These suggest that *p*-Tyr42 Rho translocation is likely upstream of β-catenin. Major β-catenin and *p*-Tyr42 Rho were apparently co-localized in nucleus upon Wnt3A stimulation, and a small portion of *p*-Tyr42 Rho and β-catenin was not co-localized in the nucleus with Wnt3A stimulation in 293 A cells of flattened large shape (Fig. 7F) in HEK293T cells (sFig. 3C). In addition to Wnt3A, hydrogen peroxide also induced nuclear localization of *p*-Tyr42 Rho in treated HEK293T cells (Fig. 7G and sFig. 3D). Contrary to *p*-Tyr42 Rho, the un-phosphorylated RhoA levels were at the basal level and not altered in human stomach cancer tissue. However, the *p*-Tyr42 Rho staining in human stomach cancer tissues revealed to be localized to the nucleus of the tumor cells by approximately 61% (Fig. 7H and sFig. 3E). Moreover, immuneofluorescence staining with *p*-Tyr42 Rho antibody in human stomach cancer tissues apparently revealed nuclear localization of *p*-Tyr42 Rho (Fig. 7I). RhoA was analyzed to be an intermediate potent level (score 4.5) of NLS as predicted by cNLS Mapper (http://nls-mapper.iab.keio.ac.jp/cgi-bin/NLS_Mapper_form.cgi), suggesting that RhoA can be localized to both the nucleus and the cytoplasm.

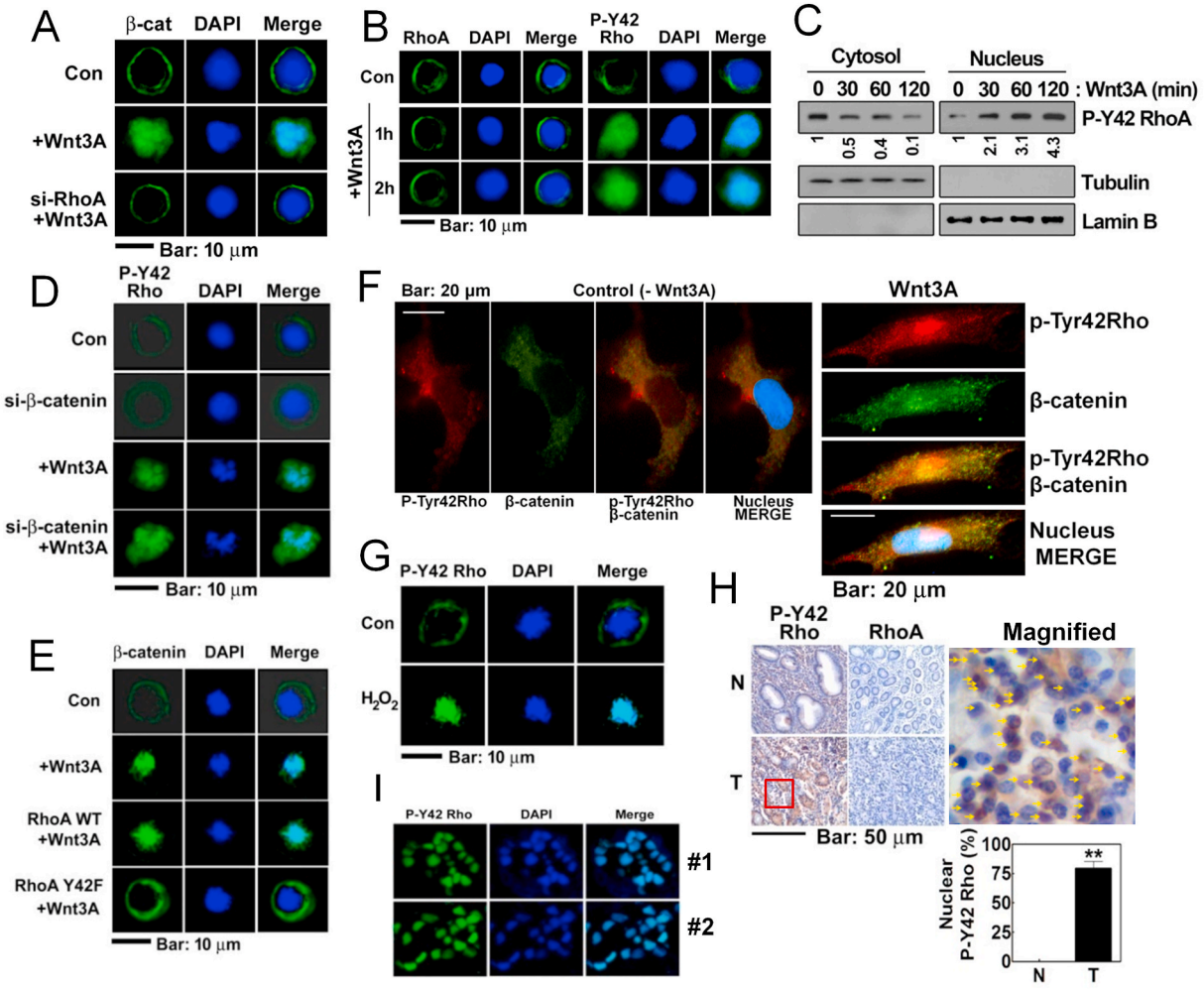

Fig. 7. *P*-Tyr42 RhoA is localized to the nucleus upon Wnt3A. (A) HEK293T cells were transfected with si-RhoA and then treated with Wnt3A (30 ng/ml) for 2 h. Localization of β-catenin was assessed by immunofluorescences assay (green) and nucleus was stained with DAPI. (B) Localization of RhoA and *p*-Tyr42 Rho were assessed in HEK293T cells stimulated by Wnt3A. (C) Cells were stimulated with Wn3A and cytosolic and nuclear *p*-Tyr42 Rho proteins were detected after each fraction preparation. (D) HEK293T cells were transfected with si-β-catenin (10 nM) for 72 h and *p*-Tyr42 Rho levels were then assessed (green). (E) HEK293T cells were transfected with RhoA WT and RhoA Y42F, then the cells were stimulated with Wnt3A, and the localization of β-catenin was assessed as above. (F) 293 A cells of flattened large shape were treated with Wnt3A (50 ng/ml) for 30 min and *p*-Tyr42 Rho (red) and β-catenin (green) were visualized with immunohistochemical method. (G) HEK293T cells were stimulated with 100 μM H_2O_2 for 2 h and localization of *p*-Tyr42 Rho was assessed. (H) Human stomach cancer tissues were stained with *p*-Tyr42 Rho antibody and the *p*-Tyr42 Rho presence in the nucleus were scored. Yellow arrows indicate cells containing nuclear *p*-Tyr42 Rho. (I) Immunofluorescence staining of human stomach cancer tissues with p-Ty42 Rho antibody was performed. (For interpretation of the references to color in this figure legend, the reader is referred to the Web version of this article.)

3.8. *p-Tyr42 Rho binds to promoters of specific genes such as Vim*

We analyzed RNA expression changes due to Wnt3A treatment and found that expression of many genes were up-regulated or down-reguated (sFig. 4A). Furthermore, expression of many genes was inhibited by si-RhoA and reconstituted RhoA Y42F, while expression of many genes was recovered to control upon Wnt3A, suggesting *p*-Tyr42 RhoA regulates expression of many genes (sFig. 4B). However, it was difficult to estimate which gene(s) is directly regulated by *p*-Tyr42 RhoA. Therein, we performed DNA sequencing after ChIP with *p*-Tyr42 Rho antibody from 4T1 cells which were stimulated by hydrogen peroxide (sFig. 5A). We identified specific genes, the promoters of which were associated with *p*-Tyr42 Rho. We selected common genes, the promoters which *p*-Tyr42 Rho binds to and which are stimulated by Wnt3A (Fig. 8A). Archive of target genes of Wnt was obtained from The Atlas of Genetics and Cytogenetics in Oncology and Haematology (http://atlasgeneticsoncology.org/Categories/WNT.html). We found *Vim* gene was one of them and selected *Vim* gene as a representative of target gene of *p*-Tyr42 Rho, because the human vimentin promoter has been reported to be also upregulated by β-catenin and TCF-4 co-transfection [41]. We presented that the promoter of *Vim* gene for vimentin was associated with *p*-Tyr42 RhoA antibody (Fig. 8B). Accordingly, we observed that DNA fragment covering promoter of *Vim* was shown to bind with *p*-Tyr42 RhoA by using PCR after ChIP with *p*-Tyr42 RhoA antibody (Fig. 8C). In addition, Wnt3A increased the expression of vimentin, *N*-cadherin and Snail, whereas that of *E*-cadherin was decreased; these all turn out to be markers of epithelial-mesenchymal transition (EMT) (Fig. 8D). We have now provided evidence that *p*-Tyr42 RhoA regulates the expression of vimentin in response to Wnt3A. Transfection with si-RhoA attenuated vimentin expression increases due to Wnt3A, but reconstituted RhoA WT restored vimentin protein expression. In contrast, transfection with RhoA Y42F, the dephospho-mimic, could not restore the vimentin expression change, suggesting that *p*-Tyr42 version of RhoA is critical for vimentin expression (Fig. 8E). To ascertain whether *p*-Tyr42 RhoA and/or β-catenin directly regulate(s) transcription of *Vim*, a *Vim*-promoter-luciferase (Luc) assay was performed. Wnt3A significantly induced the Top-flash reporter luciferase gene expression and WT RhoA slightly enhanced,

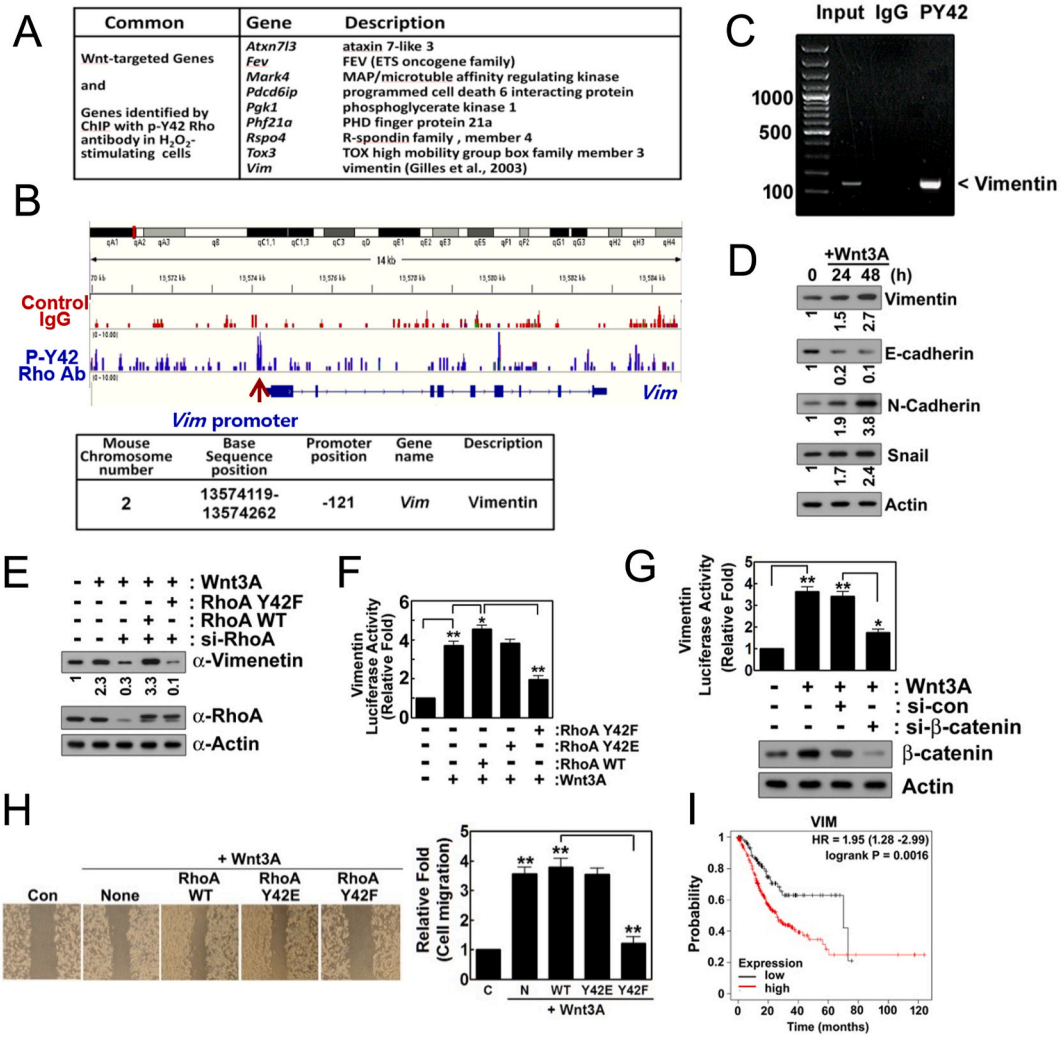

Fig. 8. *p*-Tyr42 RhoA binds to the promoter of *Vim* gene, leading to increased expression of vimentin. (A) Cells (4T1) were treated with hydrogen peroxide (100 μM) for 12 h and ChIP sequencing was performed. Common genes of Wnt-target and the promoter of which *p*-Tyr42 Rho binds to are listed. (B) *Vim* map and promoter region of *Vim*, the promoter of which *p*-Tyr42 Rho was associated with was shown. (C) 4T1 cells were stimulated with Wnt3A (30 ng/ml) for 2 h and ChIP PCR was performed with primers covering the promoter region. (D) HEK293T cells were stimulated with Wnt3A (30 ng/ml) for 2 h and maker proteins for EMT were assessed by western blotting. (E) HEK293T cells were transfected with si-RhoA for 72 h, then transfected with RhoA WT and Y42F. Expressions of vimentin and RhoA were detected by western blotting of the cell lysates. (F) HEK293T cells were transfected with RhoA WT, Y42E and Y42F DNA (4 μg) along with Vim promoter-Luc DNA for 24 h, then cells were stimulated by Wnt3A (30 ng/ml) for 2 h and luciferase activity was measured. (G) HEK293T cells were transfected with si-control and si-β-catenin (10 nM) for 72 h, then cells were stimulated by Wnt3A (30 ng/ml) for 2 h and luciferase activity was subsequently measured. (H) Migration of cells transfected with RhoA WT, Y42E and Y42F were measured. (I) Survival probability of gastric cancer patients harboring low and high *VIM* mRNA levels was obtained from Kaplan-Meier Plotter site.

whereas RhoA Y42F, dephospho-mimetic significantly reduced reporter luciferase gene expression (Fig. 8F), suggesting that *p*-Tyr42 RhoA regulates vimentin expression. As expected, si-β-catenin also abolished Vim-Luc activity in response to Wnt3A (Fig. 8G). As vimentin is a typical marker for EMT, we measured cell migration. RhoA Y42F inhibited cell migration upon Wnt3A (Fig. 8H). In addition, survival probability of human stomach cancer patients with respect to the relative expression levels of vimentin was determined. High expression of vimentin exhibited lower survival probability compared to low level of vimentin (Fig. 8I). The result was derived by using Kaplan-Meier Plotter site (https ://kmplot. com/analysis/).

3.9. Upregulation of p-Tyr42 RhoA levels in gastric cancer patients

We next assessed the relative levels *p*-Tyr42 Rho in certain human cancer types. From tissue antibody staining, cervix invasive squamous carcinoma (SCC), esophagus SCC, lung SCC, colon adenocarcinoma, stomach adenocarcinoma, liver hepatocellular carcinoma (HCC), lung SCC, and breast ductal carcinoma samples expressed higher levels of *p*-Tyr42 Rho (Fig. 9A). Moreover, *p*-Tyr42 Rho levels were remarkably increased in the more advanced cancer types with our data being focused on the stomach adenocarcinoma cases. For these cases, the patient specimens from stage III stomach adenocarcinoma revealed much stronger staining of *p*-Tyr42 Rho than in the stage I and II samples (Fig. 9B). Stomach cancer patients containing different RhoA transcription levels (mRNA levels) did not reveal dramatic different survival probability (Fig. 9C and sFig. 6B, respectively) and the mRNA expression levels of RhoA and vimentin, and survival probabilities were different depending on types of cancer (sFig. 6A and 6B) For an absolute comparison of various stomach cancer patient samples, relative levels of *p*-Tyr42 RhoA were determined via western blotting and then correlated with patient survival data (Fig. 9D–9F, and sFig. 6C for information of stomach cancer patients). *p*-Tyr42 RhoA intensity was generally increased in the more advanced stages of the cancer tumors and

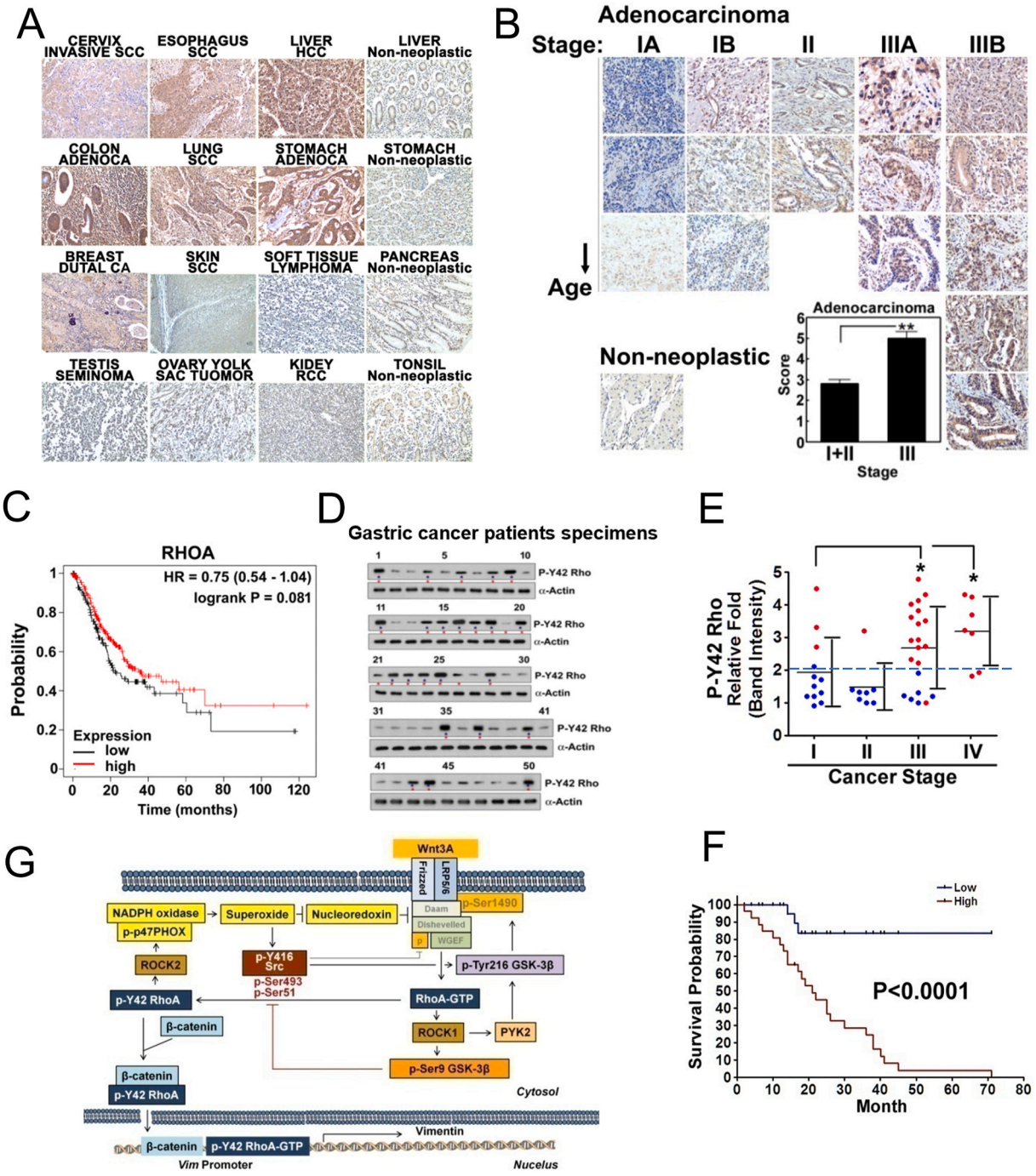

Fig. 9. Clinical outcome of *p*-Tyr42 Rho expression in human cancer patients. (A) Several cancer types from patients were stained with *p*-Tyr42 Rho antibody. (B) Several gastric cancer tissues were stained with *p*-Tyr42 Rho antibody and quantitative scoring of stages of gastric cancer tissues was performed. (C) Survival probability of gastric cancer patients harboring low and high *RhoA* mRNA levels was obtained from raw data of Kaplan-Meier Plotter site (https://kmplot.com/analysis/; Pan-cancer mRNA seq, stomach cancer). (D) *P*-Tyr42 RhoA levels of gastric cancer patient tissue specimens were analyzed by western blotting. Blue star: high level; red star: patient succumbed to cancer (died). (E) Band intensity of *p*-Tyr42 Rho levels for gastric cancer patients was plotted against their cancer stage. Red spots, patient died; blue spots, they are alive. (F) Survival probability based on the relative detected *p*-Tyr42 Rho levels from stomach cancer patients was plotted. (G) Schematic illustration of Wnt3A signaling through *p*-Tyr42 RhoA is shown. RhoA can be activated by Wnt3A likely through Daam, Dishevelled and WGEF. Activated RhoA stimulates superoxide production through p-p47PHOX. Consequently, superoxide inhibits nucleoredoxin, which suppresses Dishevelled. Superoxide activates Src kinase, which then induces phosphorylation of Tyr42 of RhoA along with Tyr216 phosphorylation of GSK-3β, which likely phosphorylates LRP5/6, leading to recruitment of the "destruction box" containing APC, Axin and GSK-3β, leading to β-catenin stabilization. *P*-Tyr42 RhoA binds to *N*-terminal of β-catenin, leading to nuclear localization of the protein complex. *P*-Tyr42 RhoA associates with the promoter of *Vim* gene along with β-catenin, resulting in increased vimentin expression, which is a typical marker of EMT. (For interpretation of the references to color in this figure legend, the reader is referred to the Web version of this article.)

surprisingly, almost patients harboring high *p*-Tyr42 RhoA level were markedly dead (Fig. 9E). Remarkably, the patients harboring higher *p*-Tyr42 RhoA GTPase levels also exhibited much worse survival probability at 5 years (60 months) (survival < 5%) compared with patients having lower *p*-Tyr42 Rho levels, (survival >85%) in Kaplan-Meier Plot (Fig. 9F). These results indicate that the higher levels of *p*-Tyr42 RhoA in stomach tumor samples are critically detrimental for survival. Taken together we propose the schematic illustration of Wnt3A signaling pathway of *p*-Tyr42 RhoA/β-catenin activation (Fig. 9G).

4. Discussion

4.1. Function of superoxide produced by Wnt3A stimulation

In the previous study, we showed that activation of RhoA is critical for β-catenin accumulation with Wnt3A stimulation [26]. Here, we showed that Wnt3A induces superoxide production through p47phox. Notably, *p*-Tyr42 RhoA preferentially bound to ROCK2, which in turn preferentially bound to p47phox, leading Ser345 phosphorylation of p47phox (Figs. 1H and 2H). Meanwhile, the oxidation of Src through intramolecular disulfide bridge between Cys245 and Cys487 upon exposure to ROS leads to Src activation [42]. Hereby, we propose this sequence of superoxide production pathway: superoxide → Src → *p*-Tyr42 RhoA → ROCK2 → p-p47phox → superoxide, a positive feed-forward loop accelerating superoxide production.

It was reported that nucleoredoxin (NRX) binds to Dishevelled (Dvl) and overexpression of NRX suppresses the Wnt-β-catenin pathway. However, hydrogen peroxide inhibited the association of Dvl and NRX [43]. Here, we verified that si-NRX enhances superoxide production upon stimulation with Wnt3A (Fig. 1K). Accordingly, superoxide produced by Wnt3A is likely to stimulate feed-forwardly Dishevelled through the inhibition of NRX (Fig. 9G).

4.2. β-Catenin accumulation through p-Tyr216 GSK-3β

In general, RhoA activated by Wnt has been known to be via the non-canonical pathway, which is not related to β-catenin [1]. However, in consistent to the previous report [26], we revealed that si-RhoA impaired β-catenin accumulation and reconstitution of RhoA restored β-catenin accumulation (Fig. 5A), suggesting that RhoA activity and β-catenin stability are very closely linked, although the underlying mechanism by which RhoA induces β-catenin accumulation in response to Wnt3A remains to be revealed.

Of note, we found that *p*-Ser9 and *p*-Tyr216 GSK-3β are concurrently induced by Wnt3A (Fig. 2D). However, it has been controversial as to whether *p*-Ser9 GSK-3β is critical for β-catenin accumulation with Wnt stimulation [44]. Some reports have described that *p*-Ser9 GSK-3β is required for β-catenin activity [45], whereas others have revealed that Wnt signaling is intact without *p*-Ser9 GSK-3β [9,10]. As such, phosphorylation of other sites such as *p*-Thr390/Ser389 of GSK-3β induced by p38 may be involved in GSK-3β inactivation and β-catenin accumulation [46]. Therein, the function of *p*-Ser9 GSK-3β in Wnt signaling pathway has not been fully elucidated.

Meanwhile, Src was reported to activate Wnt3A signaling through Tyr phosphorylation of Dishvelled and β-catenin [47]. However, the function of Src in Wnt signaling is controversial in that LRP6 phosphorylation at Tyr1460 by Src serves a negative regulatory function to prevent over-activation of Wnt signaling [48]. This discrepancy may be due to time-dependency of Src activity. Nonetheless, membrane portion of Src, which may be involved in LRP6 phosphorylation, was reduced whereas cytosolic Src was increased (Fig. 3C).

Insulin as well as Wnt3A has also been reported to concurrently induce both *p*-Ser9 and *p*-Tyr216 GSK-3β in HepG2 cells [49]. It remains controversial whether *p*-Tyr216 GSK-3β is an active kinase. *P*-Tyr216 for GSK-3β and *p*-Tyr279 for GSK-3α are required for their full GSK-3 kinase activity *in vitro* [50,51]. However, some reports revealed that Tyr216 phosphorylation of GSK-3β has no or minimal impact on GSK-3 activity *in vitro*, in a kinase assay using myelin basic protein (MBP) or tau (Ser396/404 residues) as substrates [52,53]. These results indicate that *p*-Tyr216 GSK-3β has a kinase activity towards specific favorable substrates, or that there may be different compartmental pools of *p*-Ser9 and *p*-Tyr216 GSK-3β [2]. In presence of Wnt, GSK-3β phosphorylates Ser1490 of LRP6 along with CK1 priming phosphorylation of Thr1479 in LRP6, leading to Axin binding to LRP5/6 receptor along with GSK-3β. Consequently, GSK-3β cannot interact with and phosphorylate β-catenin, resulting in increased β-catenin stability. Therein, we propose that RhoA activated by Wnt3A stimulation allows the activated *p*-Tyr216 GSK-3β to phosphorylate LRP5/6, resulting in increased β-catenin stability. Notably, *p*-Tyr216 GSK-3β was much enhanced even in peripheral regions including plasma membrane by Wnt3A stimulation, while localization of a portion of *p*-Ser9 was different from *p*-Tyr216 GSK-3β (Fig. 2I).

We speculates that RhoA-GTP/ROCK1 rather than *p*-Tyr42 RhoA/ROCK2 may favorably regulate PYK2 via its phosphorylation, in that not only RhoA WT and RhoA Y42E but RhoA Y42F, a dephospho-mimic form also induced β-catenin accumulation (Fig. 5A), and in that PYK2 is regulated by RhoA/ROCK [33], although the detail molecular mechanism by which RhoA/ROCK1 or/and *p*-Tyr42 RhoA/ROCK2 regulates PYK2 activity remains to be discovered. However, it is evident that Src also directly regulated Tyr216 phosphorylation of GSK-3β in response to Wnt stimulation (Fig. 2G).

4.3. p-Ser9 GSK-3β phosphorylates Ser43, Ser51, and Ser493 residues of src, regulating src activity

In this study, we revealed that Src was activated in early period and then inactivated in late phase upon Wnt3A (Fig. 3A). In addition, we surprisingly observed GSK-3β S9D (phospho-mimic mutant form) corresponding to *p*-Ser9 GSK-3β, which has been known to be a kinase inactive form regarding to GS, was revealed to phosphorylate Ser493 and Ser51 residues of Src along with binding with ROCK1 and *p*-Ser9 GSK-3β and reduced Tyr416 phosphorylation of Src *in vitro*, leading to Src inactivation (Fig. 3J). In contrast, the phosphorylation of Ser43 of Src caused low level of *p*-Ser of Src and reduced ROCK1 binding to Src along with an increase of *p*-Tyr416 Src, but induced Src binding with *p*-Tyr42RhoA, ROCK2, and *p*-Tyr216 GSK-3β. The regulatory mechanism of Src through Ser phosphorylation is that ROCK1 bound to Src phosphorylates Ser9 of GSK-3β, leading to phosphorylation of Ser493 and/or Ser51, along with reduced *p*-Tyr416 of Src (Fig. 3L). However, Ser43 phosphorylation by *p*-Ser9 GSK-3β induces *p*-Tyr416 Src, leading to Src activation. ROCK2 and *p*-Tyr42 RhoA bind to Src, where they transmit other signaling pathway through p-p47phox (Figs. 1H, 2G and 3L). *P*-Ser493 and *p*-Ser51 of Src is likely to be prerequisite for Ser43 phosphorylation of Src. Notably, *N*-terminal domain of Src critically regulates Src activity via specific phosphorylation at Ser51 and Ser43 along with Ser493 of *C*-terminal domain of Src in response to Wnt3A. We showed positions of Ser493 and Tyr416 in 3D Src structure, but Ser51 and Ser43 cannot be correctly indicated, because three dimensional structure of *N*-terminal region of Src could not be defined (sFig. 1D) (inactive form, PDB 2src; activated form PDB 1y57; http://proteopedia.org). We speculate that the Unique domain of Src containing Ser51 and Ser43 residues (Fig. 3H) may be localized near Ser493-contained region and *p*-Ser9 GSK-3β is able to phosphorylate in series these Ser residues. Thereby, to our knowledge, we here first propose a novel function that *p*-Ser9 GSK-3β regulates Src activities and may be a feed-back inhibitory modulator in Wnt signaling in late phase. Furthermore, other function(s) of the phosphorylation of Unique domain of Src may remain to be revealed.

4.4. Interaction of p-Tyr42 RhoA with β-catenin

Here, we found that Wnt3A also induces the complex formation of

β-catenin and RhoA, particularly p-Y42 RhoA. Also, RhoA preferentially binds to *N*-terminal domain (NTD: aa 1–140) of β-catenin (Fig. 4G). NTD and *C*-terminal domain (aa 665–781) of β-catenin may be structurally flexible while the central ARM domains (aa 141–664) forming a relatively rigid scaffold. The central region of β-catenin is known to play a role as a platform for many β-catenin-binding proteins [54]. However, both terminal regions of β-catenin (NTD and CTD) have been proposed to fold back on the central armadillo repeat. WT β-catenin cannot bind to TATA box binding protein (TBP), but the central ARM domain of β-catenin readily binds to TBP [55]. Here, we propose that *p*-Tyr42 RhoA binds to the NTD of β-catenin, suggesting that RhoA does not compete with other known partner proteins of β-catenin (Fig. 8E). Hence, RhoA binding likely enables β-catenin to bind to specific regulator protein(s). Interestingly, Snail1 as well as directly binds to NTD (aa 1–89) of β-catenin and enhances Wnt-target gene expression in a positive feed-back loop [56].

We found that p-Y42 RhoA also readily translocated to the nucleus, similarly to β-catenin, upon Wnt3A signaling (Fig. 7A). It is remarkable that RhoA Y42F (dephospho-mimetic) did not interfere with β-catenin accumulation (Fig. 5A), but RhoA Y42F could not bind to β-catenin (Fig. 5B and 5C). Moreover, RhoA Y42F impaired β-catenin activity and nuclear localization of β-catenin (Figs. 5F and 7E, respectively). Thereby, we propose that p-Y42 RhoA is able to facilitate β-catenin translocation to nucleus. However, the mechanism by which *p*-Tyr42 RhoA translocates to the nucleus remains elusive. *P*-Tyr42 Rho was also found in nucleus of the human stomach cancer cells from patient samples (Fig. 7H and 7I). Of note, in contrast to *p*-Tyr42 RhoA, Tyr34 and Tyr66 of RhoA are able to be also phosphorylated by Src, which renders RhoA to be an inactive form [40].

4.5. Function of p-Tyr42 RhoA in the nucleus

The function of β-catenin in the nucleus has been extensively studied where β-catenin binds with TCF, which then regulates transcription of specific genes in nucleus. We also tried to focus on the function of *p*-Tyr42 RhoA in the nucleus for this study. One clue for this function is that the RhoA effector protein, ROCK2, which was supposed to be activated by *p*-Tyr42 RhoA (Fig. 2H), may enhance the activation of p300 acetyltransferase by phosphorylation [57]. Thereby, it is possible that *p*-Tyr42 RhoA GTPase causes the acetylation of β-catenin through p300 acetyltransferase, remarkably enhancing β-catenin activity as a co-activator of TCF4 in the nucleus. Previously, Net1, a RhoGEF, was reported to exist in the nucleus, where it activates the nuclear RhoA. Moreover, ionizing radiation specifically promotes the activation of the nuclear pool of RhoA in a Net1-dependent manner, while the cytoplasmic RhoA activity is not affected [58]. However, we could not find significant change of nuclear RhoA by Wnt3A.

In this study, we have demonstrated an alternative possible function of *p*-Tyr42 RhoA to regulate the expression of specific genes, in particular EMT markers including increases of vimentin, *N*-cadherin and Snail, but a decrease of *E*-cadherin (Fig. 8D). Of note, β-catenin binds to Lef1 and activates Lef1 transcription complex, leading to down-regulation of *E*-cadherin expression [59]. Besides Snail, Slug and ZEB1 bind to the promoter of *E*-cadherin gene, resulting in repression of *E*-cadherin expression [60]. In particular, vimentin promoter is composed of many elements, including binding sites for activator protein-1 (AP-1), NF-κB, Smad/AP1SP1, and hypoxia induced factor-1 (HIF-1) [61–65]. For instance, HDAC1 promotes nuclear translocation of NF-κB, which binds to the promoter of *Vim* gene, thereby leading to enhanced vimentin expression [66].

In this study, as a novel mechanism, *p*-Tyr42 RhoA binds to promoter of *Vim* and regulates vimentin expression, suggesting that *p*-Tyr42 RhoA regulates EMT (Fig. 8). Since expression of vimentin can be also induced by β-catenin [41], we speculate *p*-Tyr42 RhoA binding to β-catenin facilitate vimentin expression.

Vimentin is known to be an intermediate filament protein, but it also plays a variety of other roles in cells [67]. Of note, vimentin can activate RhoA through GEF-H1 (also known as ARHGEF2) [68]. In addition, vimentin is a notable marker of EMT, and it binds to several proteins including ERK, 14-3-3, and AKT, and stabilizes proteins including Axl and Scrib for cell migration [69]. Although vimentin can be secreted to extracellular region [70], its function has not been established. From these previous reports it can be considered that *p*-Tyr42 RhoA regulates a variety of cellular functions through vimentin expression.

In addition to *p*-Tyr42 RhoA, nuclear localization/transactivation of β-catenin is regulated by several regulatory proteins including Rac1/Tiam1 [71], β-catenin Ser191 and Ser605 phosphorylation by Jun *N*-terminal kinase (JNK) [72], pyruvate kinase M2 (PKM2) in response to epithelial growth factor (EGF) [73], FoxM1 [74], importin [75], and FOXO [76]. Thus, it is likely that the nuclear translocation/activity of β-catenin is regulated by a variety of mechanisms in the context of specific signaling pathways.

p-Tyr42 Rho was shown to be upregulated in gastric cancer tissues as well as several other cancer types (Fig. 9). Furthermore, *p*-Tyr42 Rho may be a good prognostic marker for gastric cancer and a favorable target for anti-cancer intervention because gastric cancer patients with relatively high expression of Tyr42 Rho exhibited significantly lower survival probability (Fig. 9E), although a mouse study with targeting of Tyr42 Rho or its target in a gastric cancer model may be required to support this statement. Nonetheless, we demonstrated that 4T1 mouse breast cancer cells transfected with dephospho-mimic RhoA Y42F could not promote tumorigenesis in allograft experiments [18]. From Fig. 9A, *p*-Tyr42 Rho may turn out to be a critical mediator of enhancing or exacerbate several cancers.

5. Conclusion

Taken together, we propose that RhoA/ROCK is also an essential regulatory player in β-catenin accumulation and activation through ROS production and Src activation in response to Wnt3A (Figs. 1 and 2). Intriguingly, *p*-Ser9 GSK-3β induced by Wn3A can phosphorylate Ser493 and Ser51 of Src, thereby leading to Src inactivation in feed-back inhibition phase (Fig. 3M). In addition, it was demonstrated that *p*-Tyr42 RhoA directly interact with β-catenin and nuclear localization of *p*-Tyr42 RhoA is required for nuclear delivery of β-catenin. *P*-Tyr42 RhoA along with β-catenin regulates expression of specific genes such as *Vim* in the nucleus by binding to *Vim* promoter due to Wnt3A, thus possibly ensuring cancer progression (Fig. 9G). *p*-Tyr42 RhoA was a critical prognosis marker for survival in gastric cancer patients and may be a crucial target for anti-cancer intervention. *P*-Tyr42 RhoA is also closely related to the Alzheimer disease [77] and we speculate that *p*-Tyr42 RhoA plays a critical role pathogenesis in many diseases.

CRediT authorship contribution statement

Jae-Gyu Kim: and, and, Writing-original draft, Funding acquisition. **Shohel Mahmud:** and. **Jung Ki Min:** and. **Yoon-Beom Lee:** and. **Hyunbin Kim:** and. **Dong-Chul Kang:** and, and. **Hwee-Seon Park:** Investigation. **Jihye Seong:** Formal analysis. **Jae-Bong Park:** Conceptualization, and, Writing review and editing, Funding acquisition, Supervision.

Acknowledgement

This work was supported by the National Research Foundation of Korea (NRF) grant funded by the Republic of Korea (2018R1A4A1020922; 2020R1A2C1008245 to JBP; 2017R1D1A1B03029091 to JGK) and Hallym University (H20200135 toJBP). We appreciate Prof. Sang Won Suh (Department of Physiology, Hallym University) who performed critical reading this manuscript. We appreciated the cancer patient tissues which were obtained from Pusan National University Hospital (Pusan, Korea) and the survival

information of the patients which were obtained from KOSTAT (Daejeon, Korea).

Appendix ASupplementary data

Supplementary data to this article can be found online at https://doi.org/10.1016/j.redox.2020.101842.

Declaration of interests

The authors declare no competing interests.

Ethics approval and consent to participants

IRB of Hallym University approved the research plan using human-derived samples (HIRB-2019-048). All procedures followed were in accordance with the ethical standards of the responsible committee on human experimentation (institutional and national) and with the Helsinki Declaration of 1975, as revised in 2000. Informed consent was obtained from all patients for being included in the study. All institutional and national guidelines for the care and use of laboratory animals were followed.

References

[1] B.W. Doble, J.R. Woodgett, GSK-3: tricks of the trade for a multi-tasking kinase, J. Cell Sci. 116 (2003) 1175–1186.

[2] J.A. McCubrey, L.S. Steelman, F.E. Bertrand, N.M. Davis, S.L. Abrams, G. Montalto, A.B. D'Assoro, M. Libra, F. Nicoletti, R. Maestro, J. Basecke, L. Cocco, M. Cervello, A.M. Martelli, Multifaceted roles of GSK-3 and Wnt/beta-catenin in hematopoiesis and leukemogenesis: opportunities for therapeutic intervention, Leukemia 28 (2014) 15–33.

[3] J.L. Stamos, M.L. Chu, M.D. Enos, N. Shah, W.I. Weis, Structural basis of GSK-3 inhibition by N-terminal phosphorylation and by the Wnt receptor LRP6, Elife 3 (2014), e01998.

[4] D. Wu, W. Pan, GSK3: a multifaceted kinase in Wnt signaling, Trends Biochem. Sci. 35 (2010) 161–168.

[5] C. Sutherland, I.A. Leighton, P. Cohen, Inactivation of glycogen synthase kinase-3 beta by phosphorylation: new kinase connections in insulin and growth-factor signalling, Biochem. J. 296 (Pt 1) (1993) 15–19.

[6] C. Sutherland, P. Cohen, The alpha-isoform of glycogen synthase kinase-3 from rabbit skeletal muscle is inactivated by p70 S6 kinase or MAP kinase-activated protein kinase-1 in vitro, FEBS Lett. 338 (1994) 37–42.

[7] S. Song, N. Mazurek, C. Liu, Y. Sun, Q.Q. Ding, K. Liu, M.C. Hung, R.S. Bresalier, Galectin-3 mediates nuclear beta-catenin accumulation and Wnt signaling in human colon cancer cells by regulation of glycogen synthase kinase-3beta activity, Canc. Res. 69 (2009) 1343–1349.

[8] J. Chen, A.W. Chan, K.F. To, W. Chen, Z. Zhang, J. Ren, C. Song, Y.S. Cheung, P. B. Lai, S.H. Cheng, M.H. Ng, A. Huang, B.C. Ko, SIRT2 overexpression in hepatocellular carcinoma mediates epithelial to mesenchymal transition by protein kinase B/glycogen synthase kinase-3beta/beta-catenin signaling, Hepatology 57 (2013) 2287–2298.

[9] V.W. Ding, R.H. Chen, F. McCormick, Differential regulation of glycogen synthase kinase 3beta by insulin and Wnt signaling, J. Biol. Chem. 275 (2000) 32475–32481.

[10] E.J. McManus, K. Sakamoto, L.J. Armit, L. Ronaldson, N. Shpiro, R. Marquez, D. R. Alessi, Role that phosphorylation of GSK3 plays in insulin and Wnt signalling defined by knockin analysis, EMBO J. 24 (2005) 1571–1583.

[11] H. Yamanaka, T. Moriguchi, N. Masuyama, M. Kusakabe, H. Hanafusa, R. Takada, S. Takada, E. Nishida, JNK functions in the non-canonical Wnt pathway to regulate convergent extension movements in vertebrates, EMBO Rep. 3 (2002) 69–75.

[12] Y. Zhu, Y. Tian, J. Du, Z. Hu, L. Yang, J. Liu, L. Gu, Dvl2-dependent activation of Daam1 and RhoA regulates Wnt5a-induced breast cancer cell migration, PloS One 7 (2012), e37823.

[13] D.I. Strutt, U. Weber, M. Mlodzik, The role of RhoA in tissue polarity and Frizzled signalling, Nature 387 (1997) 292–295.

[14] R. Habas, I.B. Dawid, X. He, Coactivation of Rac and Rho by Wnt/Frizzled signaling is required for vertebrate gastrulation, Genes Dev. 17 (2003) 295–309.

[15] R. Habas, Y. Kato, X. He, Wnt/Frizzled activation of Rho regulates vertebrate gastrulation and requires a novel Formin homology protein Daam1, Cell 107 (2001) 843–854.

[16] H.J. Kim, J.G. Kim, M.Y. Moon, S.H. Park, J.B. Park, IkappaB kinase gamma/nuclear factor-kappaB-essential modulator (IKKgamma/NEMO) facilitates RhoA GTPase activation, which, in turn, activates Rho-associated KINASE (ROCK) to phosphorylate IKKbeta in response to transforming growth factor (TGF)-beta1, J. Biol. Chem. 289 (2014) 1429–1440.

[17] A.B. Jaffe, A. Hall, Rho GTPases: biochemistry and biology, Annu. Rev. Cell Dev. Biol. 21 (2005) 247–269.

[18] J.G. Kim, K.C. Choi, C.W. Hong, H.S. Park, E.K. Choi, Y.S. Kim, J.B. Park, Tyr42 phosphorylation of RhoA GTPase promotes tumorigenesis through nuclear factor (NF)-kappaB, Free Radic. Biol. Med. 112 (2017) 69–83.

[19] J. Liu, S. Li, S. Chen, S. Chen, Q. Geng, D. Xu, c-Met-dependent phosphorylation of RhoA plays a key role in gastric cancer tumorigenesis, J. Pathol. 249 (2019) 126–136.

[20] K. Tanegashima, H. Zhao, I.B. Dawid, WGEF activates Rho in the Wnt-PCP pathway and controls convergent extension in Xenopus gastrulation, EMBO J. 27 (2008) 606–617.

[21] Y.W. Qiang, Y. Endo, J.S. Rubin, S. Rudikoff, Wnt signaling in B-cell neoplasia, Oncogene 22 (2003) 1536–1545.

[22] S. Kishida, H. Yamamoto, A. Kikuchi, Wnt-3a and Dvl induce neurite retraction by activating Rho-associated kinase, Mol. Cell Biol. 24 (2004) 4487–4501.

[23] Y. Endo, V. Wolf, K. Muraiso, K. Kamijo, L. Soon, A. Uren, M. Barshishat-Kupper, J. S. Rubin, Wnt-3a-dependent cell motility involves RhoA activation and is specifically regulated by dishevelled-2, J. Biol. Chem. 280 (2005) 777–786.

[24] R.K. Bikkavilli, M.E. Feigin, C.C. Malbon, G alpha o mediates WNT-JNK signaling through dishevelled 1 and 3, RhoA family members, and MEKK 1 and 4 in mammalian cells, J. Cell Sci. 121 (2008) 234–245.

[25] J. Rossol-Allison, L.N. Stemmle, K.I. Swenson-Fields, P. Kelly, P.E. Fields, S. J. McCall, P.J. Casey, T.A. Fields, Rho GTPase activity modulates Wnt3a/beta-catenin signaling, Cell. Signal. 21 (2009) 1559–1568.

[26] J.G. Kim, M.J. Kim, W.J. Choi, M.Y. Moon, H.J. Kim, J.Y. Lee, J. Kim, S.C. Kim, S. G. Kang, G.Y. Seo, P.H. Kim, J.B. Park, Wnt3A induces GSK-3beta phosphorylation and beta-catenin accumulation through RhoA/ROCK, J. Cell. Physiol. 232 (2017) 1104–1113.

[27] J.G. Kim, M.Y. Moon, H.J. Kim, Y. Li, D.K. Song, J.S. Kim, J.Y. Lee, J. Kim, S. C. Kim, J.B. Park, Ras-related GTPases Rap1 and RhoA collectively induce the phagocytosis of serum-opsonized zymosan particles in macrophages, J. Biol. Chem. 287 (2012) 5145–5155.

[28] J.S. Kim, J.G. Kim, M.Y. Moon, C.Y. Jeon, H.Y. Won, H.J. Kim, Y.J. Jeon, J.Y. Seo, J.I. Kim, J. Kim, J.Y. Lee, P.H. Kim, J.B. Park, Transforming growth factor-beta1 regulates macrophage migration via RhoA, Blood 108 (2006) 1821–1829.

[29] Y. Li, J.G. Kim, H.J. Kim, M.Y. Moon, J.Y. Lee, J. Kim, S.C. Kim, D.K. Song, Y. S. Kim, J.B. Park, Small GTPases Rap1 and RhoA regulate superoxide formation by Rac1 GTPases activation during the phagocytosis of IgG-opsonized zymosans in macrophages, Free Radic. Biol. Med. 52 (2012) 1796–1805.

[30] Y. Wang, E.L. Botvinick, Y. Zhao, M.W. Berns, S. Usami, R.Y. Tsien, S. Chien, Visualizing the mechanical activation of Src, Nature 434 (2005) 1040–1045.

[31] J. Seong, S. Lu, M. Ouyang, H. Huang, J. Zhang, M.C. Frame, Y. Wang, Visualization of Src activity at different compartments of the plasma membrane by FRET imaging, Chem. Biol. 16 (2009) 48–57.

[32] F. Walker, J. deBlaquiere, A.W. Burgess, Translocation of pp60c-src from the plasma membrane to the cytosol after stimulation by platelet-derived growth factor, J. Biol. Chem. 268 (1993) 19552–19558.

[33] B.K. Yoo, P. He, S.J. Lee, C.C. Yun, Lysophosphatidic acid 5 receptor induces activation of Na(+)/H(+) exchanger 3 via apical epidermal growth factor receptor in intestinal epithelial cells, Am. J. Physiol. Cell Physiol. 301 (2011) C1008–C1016.

[34] J.A. Hartigan, W.C. Xiong, G.V. Johnson, Glycogen synthase kinase 3beta is tyrosine phosphorylated by PYK2, Biochem. Biophys. Res. Commun. 284 (2001) 485–489.

[35] C.L. Sayas, A. Ariaens, B. Ponsioen, W.H. Moolenaar, GSK-3 is activated by the tyrosine kinase Pyk2 during LPA1-mediated neurite retraction, Mol. Biol. Cell 17 (2006) 1834–1844.

[36] Y. Sun, N.H. Kim, L. Ji, S.H. Kim, J. Lee, H.J. Rhee, Lysophosphatidic acid activates beta-catenin/T cell factor signaling, which contributes to the suppression of apoptosis in H19-7 cells, Mol. Med. Rep. 8 (2013) 1729–1733.

[37] R.J. Burkhalter, S.D. Westfall, Y. Liu, M.S. Stack, Lysophosphatidic acid initiates epithelial to mesenchymal transition and induces beta-Catenin-mediated transcription in epithelial ovarian carcinoma, J. Biol. Chem. 290 (2015) 22143–22154.

[38] T. Shimizu, K. Ihara, R. Maesaki, S. Kuroda, K. Kaibuchi, T. Hakoshima, An open conformation of switch I revealed by the crystal structure of a Mg2+-free form of RHOA complexed with GDP. Implications for the GDP/GTP exchange mechanism, J. Biol. Chem. 275 (2000) 18311–18317.

[39] K. Ihara, S. Muraguchi, M. Kato, T. Shimizu, M. Shirakawa, S. Kuroda, K. Kaibuchi, T. Hakoshima, Crystal structure of human RhoA in a dominantly active form complexed with a GTP analogue, J. Biol. Chem. 273 (1998) 9656–9666.

[40] A. Uezu, H. Okada, H. Murakoshi, C.D. del Vescovo, R. Yasuda, D. Diviani, S. H. Soderling, Modified SH2 domain to phototrap and identify phosphotyrosine proteins from subcellular sites within cells, Proc. Natl. Acad. Sci. U. S. A. 109 (2012) E2929–E2938.

[41] C. Gilles, M. Polette, M. Mestdagt, B. Nawrocki-Raby, P. Ruggeri, P. Birembaut, J. M. Foidart, Transactivation of vimentin by beta-catenin in human breast cancer cells, Canc. Res. 63 (2003) 2658–2664.

[42] E. Giannoni, F. Buricchi, G. Raugei, G. Ramponi, P. Chiarugi, Intracellular reactive oxygen species activate Src tyrosine kinase during cell adhesion and anchorage-dependent cell growth, Mol. Cell Biol. 25 (2005) 6391–6403.

[43] Y. Funato, T. Michiue, M. Asashima, H. Miki, The thioredoxin-related redox-regulating protein nucleoredoxin inhibits Wnt-beta-catenin signalling through dishevelled, Nat. Cell Biol. 8 (2006) 501–508.

[44] C. Gao, G. Xiao, J. Hu, Regulation of Wnt/beta-catenin signaling by posttranslational modifications, Cell Biosci. 4 (2014) 13.

[45] S. Fukumoto, C.M. Hsieh, K. Maemura, M.D. Layne, S.F. Yet, K.H. Lee, T. Matsui, A. Rosenzweig, W.G. Taylor, J.S. Rubin, M.A. Perrella, M.E. Lee, Akt participation

in the Wnt signaling pathway through dishevelled, J. Biol. Chem. 276 (2001) 17479–17483.
[46] T.M. Thornton, G. Pedraza-Alva, B. Deng, C.D. Wood, A. Aronshtam, J.L. Clements, G. Sabio, R.J. Davis, D.E. Matthews, B. Doble, M. Rincon, Phosphorylation by p38 MAPK as an alternative pathway for GSK3beta inactivation, Science 320 (2008) 667–670.
[47] N. Yokoyama, C.C. Malbon, Dishevelled-2 docks and activates Src in a Wnt-dependent manner, J. Cell Sci. 122 (2009) 4439–4451.
[48] Q. Chen, Y. Su, J. Wesslowski, A.I. Hagemann, M. Ramialison, J. Wittbrodt, S. Scholpp, G. Davidson, Tyrosine phosphorylation of LRP6 by Src and Fer inhibits Wnt/beta-catenin signalling, EMBO Rep. 15 (2014) 1254–1267.
[49] R. Islam, J.G. Kim, Y. Park, J.Y. Cho, K.C. Cap, A.R. Kho, W.S. Chung, S.W. Suh, J. B. Park, Insulin induces phosphorylation of pyruvate dehydrogenase through RhoA activation pathway in HepG2 cells, Faseb. J. 33 (2019) 2072–2083.
[50] K. Hughes, E. Nikolakaki, S.E. Plyte, N.F. Totty, J.R. Woodgett, Modulation of the glycogen synthase kinase-3 family by tyrosine phosphorylation, EMBO J. 12 (1993) 803–808.
[51] Z.Q. Wu, T. Brabletz, E. Fearon, A.L. Willis, C.Y. Hu, X.Y. Li, S.J. Weiss, Canonical Wnt suppressor, Axin2, promotes colon carcinoma oncogenic activity, Proc. Natl. Acad. Sci. U. S. A. 109 (2012) 11312–11317.
[52] K. Itoh, T.L. Tang, B.G. Neel, S.Y. Sokol, Specific modulation of ectodermal cell fates in Xenopus embryos by glycogen synthase kinase, Development 121 (1995) 3979–3988.
[53] J.L. Buescher, C.J. Phiel, A noncatalytic domain of glycogen synthase kinase-3 (GSK-3) is essential for activity, J. Biol. Chem. 285 (2010) 7957–7963.
[54] T. Valenta, G. Hausmann, K. Basler, The many faces and functions of beta-catenin, EMBO J. 31 (2012) 2714–2736.
[55] G. Solanas, S. Miravet, D. Casagolda, J. Castano, I. Raurell, A. Corrionero, A.G. de Herreros, M. Dunach, beta-Catenin and plakoglobin N- and C-tails determine ligand specificity, J. Biol. Chem. 279 (2004) 49849–49856.
[56] V. Stemmer, B. de Craene, G. Berx, J. Behrens, Snail promotes Wnt target gene expression and interacts with beta-catenin, Oncogene 27 (2008) 5075–5080.
[57] T. Tanaka, D. Nishimura, R.C. Wu, M. Amano, T. Iso, L. Kedes, H. Nishida, K. Kaibuchi, Y. Hamamori, Nuclear Rho kinase, ROCK2, targets p300 acetyltransferase, J. Biol. Chem. 281 (2006) 15320–15329.
[58] A.D. Dubash, C. Guilluy, M.C. Srougi, E. Boulter, K. Burridge, R. Garcia-Mata, The small GTPase RhoA localizes to the nucleus and is activated by Net1 and DNA damage signals, PloS One 6 (2011), e17380.
[59] C. Jamora, R. DasGupta, P. Kocieniewski, E. Fuchs, Links between signal transduction, transcription and adhesion in epithelial bud development, Nature 422 (2003) 317–322.
[60] T. Bhatt, A. Rizvi, S.P. Batta, S. Kataria, C. Jamora, Signaling and mechanical roles of E-cadherin, Cell Commun. Adhes. 20 (2013) 189–199.
[61] M.E. Kidd, D.K. Shumaker, K.M. Ridge, The role of vimentin intermediate filaments in the progression of lung cancer, Am. J. Respir. Cell Mol. Biol. 50 (2014) 1–6.
[62] S.R. Rittling, L. Coutinho, T. Amram, M. Kolbe, AP-1/jun binding sites mediate serum inducibility of the human vimentin promoter, Nucleic Acids Res. 17 (1989) 1619–1633.
[63] A. Lilienbaum, D. Paulin, Activation of the human vimentin gene by the Tax human T-cell leukemia virus. I. Mechanisms of regulation by the NF-kappa B transcription factor, J. Biol. Chem. 268 (1993) 2180–2188.
[64] Y. Wu, X. Zhang, M. Salmon, X. Lin, Z.E. Zehner, TGFbeta1 regulation of vimentin gene expression during differentiation of the C2C12 skeletal myogenic cell line requires Smads, AP-1 and Sp1 family members, Biochim. Biophys. Acta 1773 (2007) 427–439.
[65] B. Krishnamachary, S. Berg-Dixon, B. Kelly, F. Agani, D. Feldser, G. Ferreira, N. Iyer, J. LaRusch, B. Pak, P. Taghavi, G.L. Semenza, Regulation of colon carcinoma cell invasion by hypoxia-inducible factor 1, Canc. Res. 63 (2003) 1138–1143.
[66] H. Zhou, J. Xu, C. Zhang, Y. Wen, Aberrant histone deacetylase 1 expression upregulates vimentin expression via an NF-kappaB-dependent pathway in hepatocellular carcinoma, Oncol Lett 18 (2019) 339–347.
[67] A. Satelli, S. Li, Vimentin in cancer and its potential as a molecular target for cancer therapy, Cell. Mol. Life Sci. 68 (2011) 3033–3046.
[68] Y. Jiu, J. Peranen, N. Schaible, F. Cheng, J.E. Eriksson, R. Krishnan, P. Lappalainen, Vimentin intermediate filaments control actin stress fiber assembly through GEF-H1 and RhoA, J. Cell Sci. 130 (2017) 892–902.
[69] K. Vuoriluoto, H. Haugen, S. Kiviluoto, J.P. Mpindi, J. Nevo, C. Gjerdrum, C. Tiron, J.B. Lorens, J. Ivaska, Vimentin regulates EMT induction by Slug and oncogenic H-Ras and migration by governing Axl expression in breast cancer, Oncogene 30 (2011) 1436–1448.
[70] G. Perides, C. Harter, P. Traub, Electrostatic and hydrophobic interactions of the intermediate filament protein vimentin and its amino terminus with lipid bilayers, J. Biol. Chem. 262 (1987) 13742–13749.
[71] P. Buongiorno, V.V. Pethe, G.S. Charames, S. Esufali, B. Bapat, Rac1 GTPase and the Rac1 exchange factor Tiam1 associate with Wnt-responsive promoters to enhance beta-catenin/TCF-dependent transcription in colorectal cancer cells, Mol. Canc. 7 (2008) 73.
[72] X. Wu, X. Tu, K.S. Joeng, M.J. Hilton, D.A. Williams, F. Long, Rac1 activation controls nuclear localization of beta-catenin during canonical Wnt signaling, Cell 133 (2008) 340–353.
[73] W. Yang, Y. Xia, H. Ji, Y. Zheng, J. Liang, W. Huang, X. Gao, K. Aldape, Z. Lu, Nuclear PKM2 regulates beta-catenin transactivation upon EGFR activation, Nature 480 (2011) 118–122.
[74] R.Y. Ma, T.H. Tong, A.M. Cheung, A.C. Tsang, W.Y. Leung, K.M. Yao, Raf/MEK/MAPK signaling stimulates the nuclear translocation and transactivating activity of FOXM1c, J. Cell Sci. 118 (2005) 795–806.
[75] N. Zhang, P. Wei, A. Gong, W.T. Chiu, H.T. Lee, H. Colman, H. Huang, J. Xue, M. Liu, Y. Wang, R. Sawaya, K. Xie, W.K. Yung, R.H. Medema, X. He, S. Huang, FoxM1 promotes beta-catenin nuclear localization and controls Wnt target-gene expression and glioma tumorigenesis, Canc. Cell 20 (2011) 427–442.
[76] M.A. Essers, L.M. de Vries-Smits, N. Barker, P.E. Polderman, B.M. Burgering, H. C. Korswagen, Functional interaction between beta-catenin and FOXO in oxidative stress signaling, Science 308 (2005) 1181–1184.
[77] K.C. Cap, Y.J. Jung, B.Y. Choi, S.J. Hyeon, J.G. Kim, J.K. Min, R. Islam, A. J. Hossain, W.S. Chung, S.W. Suh, H. Ryu, J.B. Park, Distinct dual roles of p-Tyr42 RhoA GTPase in tau phosphorylation and ATP citrate lyase activation upon different Abeta concentrations, Redox Biol 32 (2020) 101446.